



Obanda, A., Valerius, K., Mague, J. T., Sproules, S. and Donahue, J. P. (2020) Group 10 metal dithiolene bis(isonitrile) complexes: synthesis, structures, properties and reactivity. *Organometallics*, 39(15), pp. 2854-2870.

(doi: [10.1021/acs.organomet.0c00375](https://doi.org/10.1021/acs.organomet.0c00375))

This is the Author Accepted Manuscript.

There may be differences between this version and the published version. You are advised to consult the publisher's version if you wish to cite from it.

<https://eprints.gla.ac.uk/219946/>

Deposited on: 7 July 2020

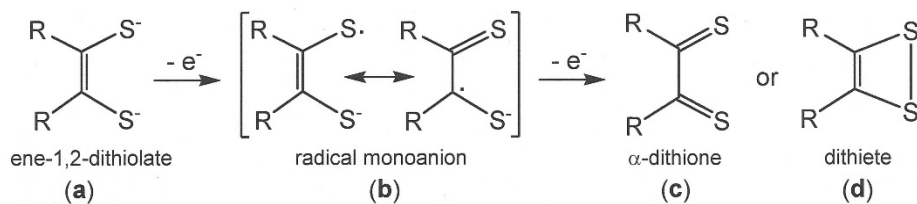
Group 10 Metal Dithiolene Bis(isonitrile) Complexes: Synthesis, Structures, Properties and Reactivity

Antony Obanda,[‡] Kendra Valerius,[‡] Joel T. Mague,[‡]
Stephen Sproules,[§] and James P. Donahue^{‡,*}

[‡]Dept. of Chemistry, Tulane University, 6400 Freret St., New Orleans, LA 70118-5698, U.S.A.

[§]WestCHEM, School of Chemistry, University of Glasgow, Glasgow, G12 8QQ, United Kingdom

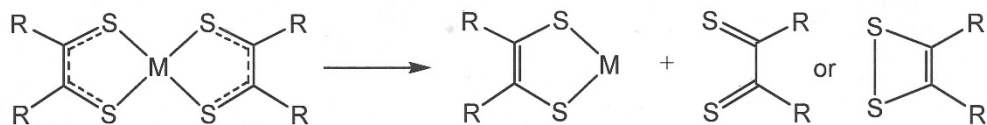
Abstract. Reaction of $[(\text{Ph}_2\text{C}_2\text{S}_2)_2\text{M}]$ ($\text{M} = \text{Ni}^{2+}, \text{Pd}^{2+}, \text{Pt}^{2+}$) with 2 eq of $\text{RN}\equiv\text{C}$ ($\text{R} = \text{Me}$ (**a**), **Bn** (**b**), **Cy** (**c**), **t**Bu (**d**), 1-Ad (**e**), **Ph** (**f**)) yields $[(\text{Ph}_2\text{C}_2\text{S}_2)_2\text{M}(\text{C}\equiv\text{NR})_2]$ ($\text{M} = \text{Ni}^{2+}$, **4a-4f**; $\text{M} = \text{Pd}^{2+}$, **5a-5f**; $\text{M} = \text{Pt}^{2+}$, **6a-6f**), which are air-stable and amenable to chromatographic purification. All members have been characterized crystallographically. Structurally, progressively greater planarity tends to be manifest as M varies from Ni to Pt, and a modest decrease in the $\text{C}\equiv\text{N}$ bond length of coordinated $\text{C}\equiv\text{NR}$ appears in moving from Ni toward Pt. Vibrational spectroscopy (CH_2Cl_2 solution) reveals $\nu_{\text{C}\equiv\text{N}}$ frequencies for $[(\text{Ph}_2\text{C}_2\text{S}_2)_2\text{M}(\text{C}\equiv\text{NR})_2]$ that are substantially higher than for free $\text{C}\equiv\text{NR}$ and increase as M ranges from Ni to Pt. This trend is interpreted as arising from increasing positive charge at M that stabilizes the linear, charge-separated resonance form of the ligand over the bent form with lowered C-N bond order. UV-vis spectra reveal lowest energy transitions that are assigned as HOMO (dithiolene π) \rightarrow LUMO (M-L σ^*) excitations. One-electron oxidations of $[(\text{Ph}_2\text{C}_2\text{S}_2)_2\text{M}(\text{C}\equiv\text{NR})_2]$ are observed at $\sim +0.5$ V due to $\text{Ph}_2\text{C}_2\text{S}_2^{2-} \rightarrow \text{Ph}_2\text{C}_2\text{S}_2^{\cdot-} + e^-$. Chemical oxidation of $[(\text{Ph}_2\text{C}_2\text{S}_2)_2\text{Pt}(\text{C}\equiv\text{N}^t\text{Bu})_2]$ with $[(\text{Br}-p\text{-C}_6\text{H}_4)_3\text{N}][\text{SbCl}_6]$ yields $[(\text{Ph}_2\text{C}_2\text{S}_2^{\cdot-})\text{Pt}(\text{C}\equiv\text{N}^t\text{Bu})_2]^{1+}$, identified spectroscopically, but in the crystalline state $[(\text{Ph}_2\text{C}_2\text{S}_2^{\cdot-})\text{Pt}(\text{C}\equiv\text{N}^t\text{Bu})_2]^{2+}$ prevails, which forms via axial $\text{Pt}\cdots\text{S}$ interactions and pyramidalization at metal. Complete substitution of MeNC from $[(\text{Ph}_2\text{C}_2\text{S}_2)_2\text{Ni}(\text{C}\equiv\text{NMe})_2]$ by 2,6-Me₂py under forcing conditions yields $[(2,6\text{-Me}_2\text{py})\text{Ni}(\mu_2\text{-}\eta^1, \eta^1\text{-S}', \eta^1\text{-S}''\text{-C}_2\text{Ph}_2)]_2$ (**8**), which features a folded Ni₂S₂ core. In most cases, isonitrile substitution from $[(\text{Ph}_2\text{C}_2\text{S}_2)_2\text{M}(\text{C}\equiv\text{NMe})_2]$ with monodentate ligands ($\text{L} = \text{phosphine}, \text{CN}^-, \text{carbene}$) typically leads to $[(\text{Ph}_2\text{C}_2\text{S}_2)_2\text{M}(\text{L})(\text{C}\equiv\text{NMe})]^n$ ($n = 0$ or 1^-), wherein $\nu_{\text{C}\equiv\text{N}}$ varies according to the relative σ donating power of L (**9** – **21**). Use of 1,3-bis(2,6-diisopropylphenyl)imidazol-2-ylidene (IPr) provides $[(\text{Ph}_2\text{C}_2\text{S}_2)_2\text{M}(\text{IPr})(\text{C}\equiv\text{NMe})]$ for $\text{M} = \text{Ni}$ (**18**) or Pd (**19**), but for Pt , attack by IPr at the isonitrile carbon occurs to yield the unusual $\eta^1, \kappa\text{C}$ -ketenimine complex $[(\text{Ph}_2\text{C}_2\text{S}_2)_2\text{Pt}(\text{C}(\text{NMe})(\text{IPr})(\text{C}\equiv\text{NMe})]$ (**20**).



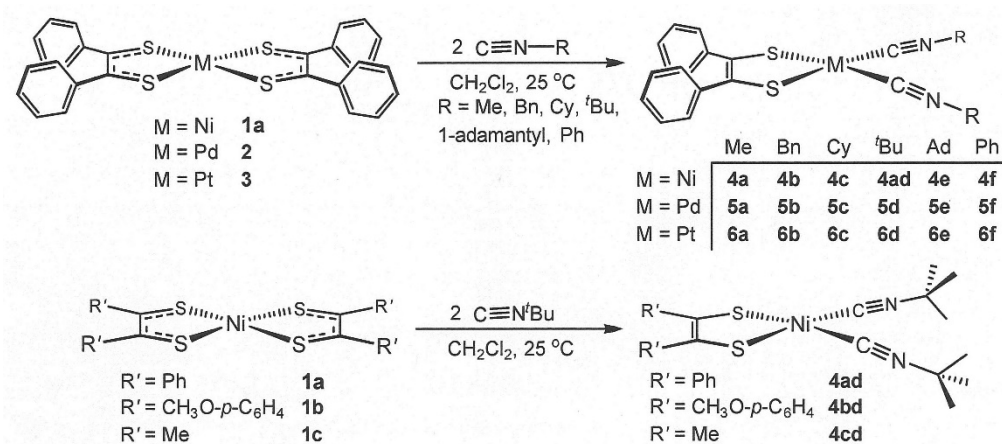
Scheme 1. Redox levels of a dithiolene ligand.

Introduction

In their charge neutral state, the bis(dithiolene) complexes of the Group 10 metals are diamagnetic species comprised of a divalent metal ion and two dithiolene ligands in a radical monoanionic state, a redox level intermediate between fully reduced ene-1,2-dithiolate and fully oxidized α -dithione or dithiete (**Scheme 1**). In the presence of a suitable reacting partner, these complexes undergo a ligand redox disproportionation whereby one of the two dithiolene ligands is extruded or transferred in an oxidized form, and the other ligand remains coordinated to M^{2+} as dithiolate dianion (**Scheme 2**). As shown, **Scheme 2** is a conceptual formalism representing a partitioning of electrons that accounts for observed products, as opposed to being a discrete reaction step itself. This ligand redox disproportionation admits of two different perspectives. On one hand, $[(R_2C_2S_2)_2M]$ complexes effectively operate as delivery agents of reactive oxidized dithiolene ligands that are otherwise not isolable and which can oxidatively add to a low-valent coordination complex, if present. The original and historically important example of this reactivity was synthesis by Schrauzer of $[(R_2C_2S_2)_2M(CO)_2]$ ($M = Mo, W$; $R = Ph, Me$).¹ These molecules have been of considerable usefulness as entry points toward small molecule analogues of the catalytic sites of molybdo- and tungstoenzymes.² Others,³⁻⁸ particularly Morris and coworkers,⁴⁻⁸ have effectively exploited this behavior for the preparation of a variety of new organometallic and inorganic transition metal complexes. In these examples, the value-added product is the coordination complex formed by oxidative addition of dithiolene ligand, while $[(R_2C_2S_2)_2M]_x$ is separated as an oligomeric or insoluble polymeric byproduct. On the other hand, if a suitable ligand L is introduced to $[(R_2C_2S_2)_2M]$, well-defined new heteroleptic dithiolene complexes of the form $[(R_2C_2S_2)ML_2]$ ($L_2 =$ two monodentate or one bidentate soft σ -donor) are efficiently produced, while the expelled oxidized dithiolene ligand is separated as ill-defined oligomer or polymer. Here again, the original example of this reaction type was described by Schrauzer, who found it to be a direct and effective route toward $[(R_2C_2S_2)M(PR_3)_2]$ complexes.^{1,9}



Scheme 2. Dithiolene ligand redox disproportionation in Group 10 bis(dithiolene) complexes. This scheme is a formalism that rationalizes products formed in reactions with other metal complexes and is not a depiction of a discrete reaction.



Scheme 3. Synthesis of Group 10 dithiolene bis(isonitrile) compounds.

As detailed in a recent account,¹⁰ we were motivated to survey the generality of dithiolene extrusion from $[(\text{R}_2\text{C}_2\text{S}_2)_2\text{M}]$ to form $[(\text{R}_2\text{C}_2\text{S}_2)\text{ML}_2]$ beyond the limited bounds of Schrauzer's work because of potential we saw for use of $[(\text{R}_2\text{C}_2\text{S}_2)\text{ML}_2]$ compounds in the targeted synthesis of complex multi-metal dithiolene complexes. The synthesis of $[(\text{Ph}_2\text{C}_2\text{S}_2)\text{M}(\text{CNR})_2]$ ($\text{M} = \text{Ni}^{2+}, \text{Pd}^{2+}, \text{Pt}^{2+}$; $\text{R} = \text{Me, Cy, }^t\text{Bu, 1-Ad, Ph}$) were disclosed in that report as well as a preliminary study of the further reactivity of $[(\text{Ph}_2\text{C}_2\text{S}_2)\text{Ni}(\text{CNMe})_2]$. In this following work, we more fully characterize the $[(\text{Ph}_2\text{C}_2\text{S}_2)\text{M}(\text{CNR})_2]$ compounds, especially structurally, and we more thoroughly lay out the panorama of outcomes when $[(\text{Ph}_2\text{C}_2\text{S}_2)\text{M}(\text{CNMe})_2]$ ($\text{M} = \text{Ni}^{2+}, \text{Pd}^{2+}, \text{Pt}^{2+}$) are introduced to new ligands intended to substitute for MeNC.

Experimental

Physical Methods: UV-vis spectra were obtained at ambient temperature with a Hewlett-Packard 8455a diode array spectrometer, while IR spectra were taken as CH_2Cl_2 solutions with a Thermo Nicolet Nexus 670 Fourier transform infrared instrument in absorption mode. All ^1H , ^{13}C and ^{31}P NMR spectra were recorded at 25°C with a Varian Unity Inova spectrometer operating at 400 MHz or with a Bruker Avance spectrometer operating at 300 MHz. Both ^1H and ^{13}C NMR spectra were referenced to the solvent signal, while an external aqueous H_3PO_4 solution was employed as reference for all ^{31}P spectra. X-band EPR spectra were recorded on a Bruker ELEXSYS E500 spectrometer, while simulations were performed with XSophe¹¹ distributed by Bruker Biospin GmbH. Mass spectrometry (MS) spectra (matrix-assisted laser desorption ionization – time of flight, MALDI-TOF) were obtained with a Bruker Autoflex III instrument operating in positive ion mode. Electrochemical measurements were made with a CHI 620C electroanalyzer workstation using a Ag/AgCl reference electrode, a glassy carbon disk working electrode, a Pt wire auxiliary electrode, and $[\text{Bu}_4\text{N}][\text{PF}_6]$ as supporting electrolyte. Typical scan rates were 50 or 100 mV/sec. Under these conditions, the $\text{Cp}_2\text{Fe}^+/\text{Cp}_2\text{Fe}$ couple consistently occurred at +540 mV. Elemental

analyses were performed by Midwest Microlab, LLC (Indianapolis, IN), Galbraith Laboratories, Inc. (Knoxville, TN), or by Kolbe Microanalytical Laboratory (Oberhausen, Germany). Details regarding the collection of X-ray diffraction data and the solving and refining of crystal structures are deferred to supporting information.

Syntheses. The $[(\text{Ph}_2\text{C}_2\text{S}_2)_2\text{M}]$, ($\text{M} = \text{Ni}^{2+}, \text{Pd}^{2+}, \text{Pt}^{2+}$) starting materials were synthesized following the procedure outlined by Schrauzer and Mayweg.¹ Methyl isonitrile was made by the dehydration of *N*-methylformamide,¹² and its density was experimentally determined to be 0.78 g/mL, while *tert*-butyl-isonitrile ($d. = 0.74$ g/mL) and phenyl isonitrile ($d. = 0.98$ g/mL)¹³ were synthesized via the phase-transfer Hofmann-carbylamine reaction.¹⁴ Cyclohexyl isonitrile ($d. = 0.878$ g/mL), 1-adamantyl isonitrile, benzyl isonitrile ($d. = 0.962$ g/mL), and $[\text{Et}_4\text{N}][\text{CN}]$ were used as received from commercial sources. Tetraisopropylbenzobisimidazolium dibromide was prepared following a published procedure¹⁵ and deprotected by a modification of the protocol by Bantreil and Nolan.¹⁶ The $[\text{BF}_4]^-$ salt of $[\text{IPr-H}]^+$ (IPr = 1,3-bis(2,6-diisopropylphenyl)imidazol-2-ylidene) was prepared and unmasked under N_2 following the same protocol reported by Bantreil and Nolan.¹⁶ The free IPr ligand was stored in a glovebox. A published procedure was also implemented for the synthesis of *p*-phenylenebis(diphenylphosphine) (1,4-dppb).¹⁷ Column chromatography separations were carried out using 63 – 200 μm silica (Dynamic Adsorbents) or 150 mesh neutral alumina (Aldrich). The solvents used for reactions were either dried with a system of drying columns from the Glass Contour Company (CH_2Cl_2 , THF), freshly distilled according to standard procedures¹⁸ (MeCN), or used as received from commercial suppliers. All reactions were conducted under an inert atmosphere of either N_2 or Ar. Subsequent purification by chromatography and crystallization were done in the open air, except where noted otherwise.

$[(\text{Ph}_2\text{C}_2\text{S}_2)\text{Ni}(\text{CNBn})_2]$, **4b.** Benzyl isocyanide (0.040 mL, $d. = 0.962$ g/mL, 0.33 mmol) was delivered dropwise via a gas-tight syringe to a solution of $[(\text{Ph}_2\text{C}_2\text{S}_2)_2\text{Ni}]$ (0.100 g, 0.184 mmol) in CH_2Cl_2 (20 mL). The mixture was stirred at 25° C for 5 h, after which time the solvent was removed under reduced pressure. The dark blue solid residual was applied directly to the top of a silica gel column packed as a slurry in hexanes. Flash elution with 1:1 CH_2Cl_2 :hexanes moved a green band of unreacted $[(\text{Ph}_2\text{C}_2\text{S}_2)_2\text{Ni}]$ followed by a well resolved blue band of **4b**. This blue fraction was collected using 2:1 CH_2Cl_2 :hexanes and taken to dryness under reduced pressure. The solid residue was washed with *n*-pentane (5 mL), redissolved in a minimal volume of CH_2Cl_2 , filtered through a Celite pad and taken to dryness again. Crystallization was accomplished by slow diffusion of hexanes vapor into a concentrated 1,2-dichloroethane solution. Yield: 0.089 g. $R_f = 0.39$ (2:1 CH_2Cl_2 :hexanes). ^1H NMR (δ , ppm in CD_2Cl_2): 7.46-7.35 (overlapping m, 10H, Bn, aromatic C–H), 7.19-7.09 (overlapping m, 10H, aromatic C–H), 4.88 (s, 4H, CH_2). ^{13}C NMR (δ , ppm in CD_2Cl_2): 142.1, 138.6, 131.7, 130.1, 129.6, 129.3, 128.0, 127.2, 126.5, 48.7 (CH_2). IR (CH_2Cl_2 , cm^{-1}): 2213 (vs, CN_{sym}), 2197 (vs, CN_{asym}). UV-vis absorption spectrum [CH_2Cl_2 , λ_{max} , nm (ϵ_{M} , $\text{M}^{-1} \text{cm}^{-1}$): 460 (400),

608 (420). Cyclic voltammetry (CV): **4b** – e⁻ → [**4b**]¹⁺, +0.50 V. Anal. Calcd for C₃₀H₂₄N₂S₂Ni: C, 67.31; H, 4.52; N, 5.23. Found: C, 67.18; H, 4.67; N, 5.21.

[(Ph₂C₂S₂)Ni(CNCy)₂], **4c**. The same procedures and scale used in the synthesis of **4b** were employed but with 0.05 mL (0.40 mmol) of cyclohexylisocyanide. Ultimately, dark purple crystals of **4c** were obtained. Yield: 0.082 g, 95%. R_f = 0.52 (2:1 CH₂Cl₂:hexanes). ¹H NMR (δ, ppm in CD₂Cl₂): 7.17–7.08 (overlapping m, 10H, aromatic C–H), 3.90 (m, 2H, Cy -CHNC), 1.94–1.89 (m, 4H, Cy), 1.81–1.73 (m, 8H, Cy), 1.54–1.46 (m, 8H, Cy). ¹³C NMR (δ, ppm in CD₂Cl₂): 142.4, 138.4, 135.9 (t), 130.1, 127.9, 126.3, 55.4 (Cy, CH), 32.4 (Cy, CH₂), 25.2 (Cy, CH₂), 22.9 (Cy, CH₂). IR (CH₂Cl₂, cm⁻¹): 2204 (vs, CN_{sym}), 2189 (vs, CN_{asym}). UV-vis absorption spectrum [CH₂Cl₂, λ_{max}, nm (ε_M, M⁻¹ cm⁻¹): 440 (240), 601 (420). MALDI MS. Calcd for C₂₈H₃₂N₂S₂Ni: *m/z* 519.401. Observed: *m/z* 519.042. Cyclic voltammetry: **4c** – e⁻ → [**4c**]¹⁺, +0.56 V. Anal. Calcd for C₂₈H₃₂N₂S₂Ni: C, 64.74; H, 6.22; N, 5.39. Found: C, 64.86; H, 5.95; N, 5.43.

[(Ph₂C₂S₂)Ni(CN^tBu)₂], **4ad**. 0.040 mL (d. = 0.74 g/mL, 0.36 mmol) of *tert*-butylisocyanide was delivered dropwise via a gas-tight syringe to a solution of **1a** (0.100 g, 0.184 mmol), in CH₂Cl₂ (25 mL) under an Ar atmosphere. Subsequent work-up and purification were as described for **4b**. Crystallization was accomplished by slow diffusion of Et₂O vapor into a concentrated CH₂Cl₂ solution to ultimately give dark blue crystals of **4ad**. Yield: 0.067 g, 81%. R_f = 0.46 (2:1 CH₂Cl₂:hexanes). ¹H NMR (δ, ppm in CD₂Cl₂): 7.16–7.14 (m, 4H, aromatic C–H), 7.12–7.09 (m, 6H, aromatic C–H), 1.53 (s, 18H, ^tBu). ¹³C NMR (δ, ppm in CD₂Cl₂): 141.8, 138.0, 135.1 (t), 129.9, 127.6, 126.0, 58.3 (t, ^tBu *tert*-C), 30.4 (^tBu CH₃). IR (CH₂Cl₂, cm⁻¹): 2197 (vs, CN_{sym}), 2180 (vs, CN_{asym}). UV-Vis absorption spectrum [CH₂Cl₂, λ_{max}, nm (ε_M, M⁻¹ cm⁻¹): ~424 (260), 600 (410). Cyclic voltammetry: **4ad** – e⁻ → [**4ad**]¹⁺, +0.59 V. Anal. Calcd for C₂₄H₂₈N₂S₂Ni: C, 61.68; H, 6.04; N, 5.99. Found: C, 61.91; H, 6.04; N, 6.08.

[(MeO-*p*-C₆H₄)₂C₂S₂)Ni(CN^tBu)₂], **4bd**. Two eq of *tert*-butylisocyanide (0.03 mL, d. = 0.74 g/mL, 0.27 mmol) were added via syringe to a solution of [(MeO-*p*-C₆H₄)₂C₂S₂)₂Ni] (0.100 g, 0.151 mmol) in CH₂Cl₂ (25 mL). Subsequent steps in work-up and purification were analogous to those described for compound **4b**; dark blue crystals of **4bd** were ultimately obtained. Yield: 0.069 g, 98%. R_f = 0.37 (2:1 CH₂Cl₂:hexanes). ¹H NMR (δ, ppm in CD₂Cl₂): 7.11–7.06 (m, 2H, aromatic C–H), 6.69–6.64 (m, 2H, aromatic C–H), 3.73 (s, 6H, –OCH₃), 1.53 (s, 18H, ^tBu). ¹³C NMR (δ, ppm in CDCl₃): 157.9, 136.8, 134.9, 131.1, 113.1, 58.2 (^tBu *tert*-C), 55.3 (–OCH₃), 30.3 (^tBu CH₃). IR (CH₂Cl₂, cm⁻¹): 2196 (vs, CN_{sym}), 2180 (vs, CN_{asym}). UV-vis absorption spectrum [CH₂Cl₂, λ_{max}, nm (ε_M, M⁻¹ cm⁻¹): 420 (200), 607 (320). MALDI MS. Calcd for C₂₆H₃₂N₂O₂S₂Ni: *m/z* 527.378. Observed: *m/z* 527.071. Cyclic voltammetry: **4bd** – e⁻ → [**4bd**]¹⁺, +0.50 V. Anal. Calcd for C₂₆H₃₂N₂O₂S₂Ni: C, 59.21; H, 6.13; N, 5.31; S, 12.16. Found: C, 59.06; H, 6.05; N, 5.36; S, 12.01.

[(Me₂C₂S₂)Ni(CN^tBu)₂], **4cd**. Neat *tert*-butylisocyanide (0.19 mL, 1.70 mmol) was delivered via syringe to a solution of [(Me₂C₂S₂)₂Ni] (0.251 g, 0.85 mmol) in CH₂Cl₂ (25 mL). The remaining synthesis and

purification steps were analogous to those employed for compound **4b**. Crystallization was achieved by diffusing hexanes into a concentrated toluene solution of **4cd** with a few drops of *tert*-butylisocyanide added in the inner vial. Yield: 0.086 g, 30%. $R_f = 0.37$ (2:1 CH₂Cl₂:hexanes). ¹H NMR (δ , ppm in CD₂Cl₂): 1.95 (s, 6H, -CH₃), 1.50 (s, 18H, ^tBu). ¹³C NMR (δ , ppm in CDCl₃): 135.8, 130.6, 58.4 (^tBu *tert*-C), 30.4 (isonitrile -CH₃), 20.7 (dithiolene -CH₃). IR (CH₂Cl₂, cm⁻¹): 2196 (vs, CN_{sym}), 2177 (vs, CN_{asym}). UV-vis absorption spectrum [CH₂Cl₂, λ_{max} , nm (ϵ_M , M⁻¹·cm⁻¹): 350 (6400), 450 (290), 614 (170). Cyclic voltammetry: **4cd** - e⁻ → [**4cd**]¹⁺, +0.42 V.

[(Ph₂C₂S₂)Ni(CN-1-Ad)₂], **4e**. Solid 1-adamantylisocyanide (0.054 g, 0.331 mmol) was added to a solution of **1** (0.090 mg, 0.166 mmol) in CH₂Cl₂ (25 mL). Subsequent steps in workup and purification procedure were similar to those implemented for **4b**, ultimately yielding dark blue crystals of **4e**. Yield: 0.076 g, 74%. $R_f = 0.64$ (2:1 CH₂Cl₂:hexanes). ¹H NMR (δ , ppm in CD₂Cl₂): 7.16-7.08 (overlapping m, 10H, aromatic C-H), 2.13 (m, 6H, adamantyl C-H), 2.10 (m, 12H, adamantyl C-H), 1.70 (m, 12H, adamantyl C-H). ¹³C NMR (δ , ppm in CD₂Cl₂): 142.4, 138.4, 134.5 (t), 130.1, 127.9, 126.3, 58.6, 43.3, 35.6, 29.3. IR (CH₂Cl₂, cm⁻¹): 2196 (vs, CN_{sym}), 2175 (vs, CN_{asym}). UV-vis absorption spectrum [CH₂Cl₂, λ_{max} , nm (ϵ_M , M⁻¹·cm⁻¹): 437 (180), 599 (360). Cyclic voltammetry: **4e** - e⁻ → [**4e**]¹⁺, +0.57 V. Anal. Calcd for C₃₆H₄₀N₂S₂Ni: C, 69.34; H, 6.47; N, 4.49. Found: C, 69.22; H, 6.33; N, 4.54.

[(Ph₂C₂S₂)Ni(CNPh)₂], **4f**. The procedure followed for the synthesis of **4b** was employed using 0.080 mL (0.76 mmol) of phenylisocyanide, which was added to a solution of [(Ph₂C₂S₂)₂Ni] (0.220 g, 0.405 mmol) in CH₂Cl₂ (25 mL). Subsequent work-up and purification steps were the same as for **4b**. Diffraction-quality green crystals of **4f** were obtained upon recrystallization. Yield: 0.143 g, 70%. $R_f = 0.63$ (2:1 CH₂Cl₂:hexanes). ¹H NMR (δ , ppm in CD₂Cl₂): 7.53-7.48 (overlapping m, 10H, aromatic C-H), 7.23-7.21 (m, 4H, aromatic C-H), 7.16-7.13 (m, 6H, aromatic C-H). ¹³C NMR (δ , ppm in CD₂Cl₂): 142.0, 139.2, 130.8, 130.2, 128.0, 126.9, 126.7. IR (CH₂Cl₂, cm⁻¹): 2182 (vs, CN_{sym}), 2162 (vs, CN_{asym}). UV-vis absorption spectrum [CH₂Cl₂, λ_{max} , nm (ϵ_M , M⁻¹·cm⁻¹): 466 (1400), 639 (480). MALDI MS. Calcd for C₂₈H₂₀N₂S₂Ni: m/z 507.306. Observed: m/z 507.003. Cyclic voltammetry: **4f** - e⁻ → [**4f**]¹⁺, +0.62 V. Anal. Calcd for C₂₈H₂₀N₂S₂Ni: C, 69.29; H, 3.97; N, 5.52. Found: C, 66.26; H, 3.87; N, 5.56.

[(Ph₂C₂S₂)Pd(CNMe)₂], **5a**. The same procedures and scale used in the synthesis of **4b** were employed but with **2** and 0.020 mL (0.38 mmol) of methylisocyanide. Ultimately, reddish-orange diffraction quality crystals of **5a** were obtained. Yield: 0.050 g, 78%. $R_f = 0.11$ (2:1 CH₂Cl₂:hexanes). ¹H NMR (δ , ppm in CD₂Cl₂): 7.16-7.08 (overlapping m, 10H, aromatic C-H), 3.45 (s, 6H, CNCH₃). ¹³C NMR (δ , ppm in CD₂Cl₂): 145.7, 137.3, 132.7, 130.8, 129.2, 33.4 (isonitrile -CH₃). IR (CH₂Cl₂, cm⁻¹): 2246 (vs, CN_{sym}), 2230 (vs, CN_{asym}). UV-vis absorption spectrum [CH₂Cl₂, λ_{max} , nm (ϵ_M , M⁻¹·cm⁻¹): 421 (690), 502 (530). Cyclic voltammetry: **5a** - e⁻ → [**5a**]¹⁺, +0.61 V. Anal. Calcd for C₁₈H₁₆N₂S₂Pd: C, 50.17; H, 3.75; N, 6.50. Found: C, 49.12; H, 3.86; N, 6.48.

[(Ph₂C₂S₂)Pd(CNBn)₂], **5b**. The same procedures and scale used in the synthesis and purification of **4b** were employed with **2** and 0.040 mL (0.33 mmol) of benzyisonitrile. Diffraction-quality red crystals of **5b** were obtained. Yield: 0.057 g, 60%. R_f = 0.35 (2:1 CH₂Cl₂:hexanes). ¹H NMR (δ, ppm in CD₂Cl₂): 7.45–7.36 (overlapping m, 10H, Bn aromatic C–H), 7.17–7.07 (overlapping m, 10H, aromatic C–H), 4.92 (s, 4H, –CH₂–). ¹³C NMR (δ, ppm in CD₂Cl₂): 143.1, 135.1, 131.3, 130.3, 129.7, 129.4, 127.9, 127.3, 126.4, 48.5 (–CH₂C₆H₅). Solution IR (CH₂Cl₂, cm⁻¹): 2227 (vs, CN_{sym}), 2213 (vs, CN_{asym}). UV-Vis absorption spectrum [CH₂Cl₂, λ_{max}, nm (ε_M, M⁻¹·cm⁻¹): 427 (150), 518 (50). MALDI MS. Calcd for C₃₀H₂₄N₂S₂Pd: *m/z* 583.086. Observed: *m/z* 582.733. Cyclic voltammetry: **5b** – e⁻ → [**5b**]¹⁺, +0.56 V. Anal. Calcd for C₃₀H₂₄N₂S₂Pd: C, 61.80; H, 4.15; N, 4.80; S, 11.00. Found: C, 61.20; H, 4.06; N, 4.75; S, 10.62.

[(Ph₂C₂S₂)Pd(CNCy)₂], **5c**. 0.040 mL (0.32 mmol) of cyclohexylisonitrile was added to a solution of **2** (0.087 g, 0.147 mmol) in CH₂Cl₂ (25 mL). The remaining synthesis and purification steps were analogous to those used for **4b**; ultimately, red crystals of **5c** were produced. Yield: 0.067 g, 73%. R_f = 0.51 (2:1 CH₂Cl₂:hexanes). ¹H NMR (δ, ppm in CD₂Cl₂): 7.17–7.07 (overlapping m, 10H, aromatic C–H), 3.96 (br m, 2H, Cy), 1.93 (m, ~4H, Cy) 1.85–1.78 (overlapping m, ~8H, Cy), 1.45–1.50 (m, ~8H, Cy). ¹³C NMR (δ, ppm in CD₂Cl₂): 143.3, 135.0, 130.3, 127.8, 126.3, 55.3, 32.3, 25.2, 22.9. IR (CH₂Cl₂, cm⁻¹): 2217 (vs, CN_{sym}), 2203 (vs, CN_{asym}). UV-vis absorption spectrum [CH₂Cl₂; λ_{max}, nm (ε_M, M⁻¹·cm⁻¹): 431 (430), 504 (490). Cyclic voltammetry (CV): **5c** – e⁻ → [**5c**]¹⁺, +0.61 V. Anal. Calcd for C₂₈H₃₂N₂S₂Pd: C, 59.30; H, 5.69; N, 4.94. Found: C, 59.47; H, 5.99; N, 4.88.

[(Ph₂C₂S₂)Pd(CN-1-Ad)₂], **5e**. The same procedures and scale used in the synthesis of **4b** were employed with **2** and 0.055 g (0.34 mmol) of 1-adamantylisonitrile. Diffraction-quality, red crystals of **5e** were obtained. Yield: 0.062 g, 55%. R_f = 0.61 (2:1 CH₂Cl₂:hexanes). ¹H NMR (δ, ppm in CD₂Cl₂): 7.17–7.07 (overlapping m, 10H, aromatic C–H), 2.13 (overlapping m, 18H, Ad), 1.71 (overlapping m, 12H, Ad). ¹³C NMR (δ, ppm in CD₂Cl₂): 143.4, 135.0, 130.3, 127.8, 126.3, 58.7, 43.2, 36.0, 29.3. IR (CH₂Cl₂, cm⁻¹): 2211 (vs, CN_{sym}), 2198 (vs, CN_{asym}). UV-vis absorption spectrum [CH₂Cl₂; λ_{max}, nm (ε_M, M⁻¹·cm⁻¹): 430 (320), 505 (420). Cyclic voltammetry: **5e** – e⁻ → [**5e**]¹⁺, +0.59 V. Anal. Calcd for C₃₆H₄₀N₂S₂Pd: C, 64.41; H, 6.01; N, 4.17. Found: C, 61.86; H, 6.08; N, 3.69.

[(Ph₂C₂S₂)Pd(CNPh)₂], **5f**. Phenylisonitrile (0.040 mL, 0.38 mmol) was added to a solution of **2** (0.120 g, 0.203 mmol), in CH₂Cl₂ (25 mL). The remaining synthesis and purification steps were analogous to those implemented for compound **4b**, yielding red crystals of **5f**. Yield: 0.070 g, 66%. R_f = 0.59 (2:1 CH₂Cl₂:hexanes). ¹H NMR (δ, ppm in CD₂Cl₂): 7.58–7.48 (overlapping m, 10H, aromatic C–H), 7.21–7.19 (m, 4H, aromatic C–H), 7.14–7.11 (m, 6H, aromatic C–H). IR (CH₂Cl₂, cm⁻¹): 2198 (vs, CN_{sym}), 2182 (vs, CN_{asym}). UV-vis absorption spectrum [CH₂Cl₂, λ_{max}, nm (ε_M, M⁻¹·cm⁻¹): ~385 (5180), ~534 (770). Cyclic voltammetry: **5f** – e⁻ → [**5f**]¹⁺, +0.67 V.

[(Ph₂C₂S₂)Pt(CNMe)₂], **6a**. The same procedures and scale used in the synthesis and purification of **4b** were employed but with **3** and methylisonitrile (0.020 mL, 0.38 mmol). Ultimately, yellow crystals were obtained upon recrystallization by diffusion of Et₂O into a concentrated CH₂Cl₂ solution of **6a**. Yield: 0.032 g, 42%. R_f = 0.14 (2:1 CH₂Cl₂:hexanes). ¹H NMR (δ, ppm in CD₂Cl₂): 7.19–7.09 (unresolved m, 10H, aromatic C–H), 3.42 (s, 6H, CNCH₃). ¹³C NMR (δ, ppm in CD₂Cl₂): 142.9, 135.2, 130.4, 127.9, 126.4, 30.5 (isonitrile –CH₃). IR (CH₂Cl₂, cm⁻¹): 2248 (vs, CN_{sym}), 2223 (vs, CN_{asym}). UV-vis absorption spectrum [CH₂Cl₂, λ_{max}, nm (ε_M, M⁻¹·cm⁻¹): 337 (4780). MALDI MS. Calcd for C₁₈H₁₆N₂S₂Pt: *m/z* 519.554. Observed: *m/z* 519.858. Cyclic voltammetry: **6a** – e⁻ → [**6a**]¹⁺, +0.64 V. Anal. Calcd for C₁₈H₁₆N₂S₂Pt: C, 41.61; H, 3.11; N, 5.39. Found: C, 41.54; H, 2.92; N, 5.44.

[(Ph₂C₂S₂)Pt(CNBn)₂], **6b**. 0.070 mL (0.58 mmol) of benzylisonitrile was added to a solution of **3** (0.200 g, 0.294 mmol) in CH₂Cl₂ (20 mL). The rest of the synthesis and purification procedures were analogous to those used for compound **4b**, yielding yellow crystals of **6b**. Yield: 0.073 g, 38%. R_f = 0.35 (2:1 CH₂Cl₂:hexanes). ¹H NMR (δ, ppm in CD₂Cl₂): 7.50–7.40 (overlapping m, 10H, aromatic C–H), 7.23–7.12 (overlapping m, 10H, aromatic C–H), 4.98 (s, 4H, –CH₂C₆H₅). ¹³C NMR (δ, ppm in CD₂Cl₂): 142.9, 135.4, 131.5, 130.5, 129.7, 129.4, 127.9, 127.3, 126.5, 48.8 (–CH₂C₆H₅). IR (CH₂Cl₂, cm⁻¹): 2229 (vs, CN_{sym}), 2204 (vs, CN_{asym}). UV-vis absorption spectrum [CH₂Cl₂, λ_{max}, nm (ε_M, M⁻¹·cm⁻¹): 342 (1560). Cyclic voltammetry: **6b** – e⁻ → [**6b**]¹⁺, +0.57 V. Anal. Calcd for C₃₀H₂₄N₂S₂Pt: C, 53.64; H, 3.61; N, 4.17; S, 9.54. Found: C, 53.49; H, 3.53; N, 4.13; S, 9.36.

[(Ph₂C₂S₂)Pt(CNCy)₂], **6c**. Cyclohexylisonitrile (0.070 mL, 0.56 mmol) of cyclohexylisonitrile was added to a solution of **3** (0.203 g, 0.299 mmol) in CH₂Cl₂ (25 mL). The remaining synthesis and purification steps were analogous to those used for compound **4b**, yielding yellow crystals of **6c**. Yield: 0.084 g, 46%. R_f = 0.47 (2:1 CH₂Cl₂:hexanes). ¹H NMR (δ, ppm in CD₂Cl₂): 7.19–7.08 (overlapping m, 10H, aromatic C–H), 4.02–3.98 (m, 2H, Cy), 1.97–1.93 (m, 4H, Cy), 1.90–1.75 (overlapping m, 8H, Cy), 1.51–1.46 (m, 8H, Cy). ¹³C NMR (δ, ppm in CD₂Cl₂): 143.1, 135.3, 130.5, 127.8, 126.3, 56.0, 32.3, 25.2, 23.0. IR (CH₂Cl₂, cm⁻¹): 2219 (vs, CN_{sym}), 2196 (vs, CN_{asym}). UV-vis absorption spectrum [CH₂Cl₂, λ_{max}, nm (ε_M, M⁻¹·cm⁻¹): 336 (9970). Cyclic voltammetry: **6c** – e⁻ → [**6c**]¹⁺, +0.67 V. Anal. Calcd for C₂₆H₃₂N₂S₂Pt: C, 51.27; H, 4.93; N, 4.27. Found: C, 51.19; H, 4.83; N, 4.23.

[(Ph₂C₂S₂)Pt(CN^tBu)₂], **6d**. The same synthesis and purification procedures used in the preparation of **4b** were employed but with 0.033 mL (0.29 mmol) of *tert*-butylisonitrile and 0.100 g (0.147 mmol) of **3**. Ultimately, yellow crystals of **6d** were obtained upon recrystallization by diffusion of hexanes vapor into a 1,2-dichloroethane. Yield: 0.036 g, 41%. R_f = 0.40 (2:1 CH₂Cl₂:hexanes). ¹H NMR (δ, ppm in CD₂Cl₂): 7.16–7.08 (overlapping m, 10H, aromatic C–H), 1.58 (s, 18H, ^tBu). IR (CH₂Cl₂, cm⁻¹): 2214 (vs, CN_{sym}), 2188 (vs, CN_{asym}). UV-vis absorption spectrum [CH₂Cl₂, λ_{max}, nm (ε_M, M⁻¹·cm⁻¹): 336 (10290). Cyclic

voltammetry: $6d - e^- \rightarrow [6d]^{1+}$, +0.66 V. Anal. Calcd for $C_{24}H_{28}N_2S_2Pt$: C, 47.75; H, 4.67; N, 4.64. Found: C, 48.09; H, 4.77; N, 4.78.

[(Ph₂C₂S₂)Pt(CN-1-Ad)₂], 6e. To a solution of **3** (0.150 g, 0.221 mmol) in CH₂Cl₂ (25 mL) was added 0.716 g (0.441 mmol) of 1-adamantylisonitrile. Subsequent handling and purification procedures were similar to those implemented for compound **4b**, ultimately yielding yellow crystals of **6e**. Yield: 0.087 g, 52%. *R_f* = 0.60 (2:1 CH₂Cl₂:hexanes). ¹H NMR (δ, ppm in CD₂Cl₂): 7.18–7.14 (m, 4H, aromatic C–H), 7.12–7.08 (m, 6H, aromatic C–H), 2.36 (m, 18H, Ad), 1.72 (m, 12H, Ad). IR (CH₂Cl₂, cm⁻¹): 2212 (vs, CN_{sym}), 2192 (vs, CN_{asym}). UV-vis absorption spectrum [CH₂Cl₂, λ_{max}, nm (ε_M, M⁻¹ cm⁻¹): 336 (6850). Calcd for C₃₆H₄₀N₂S₂Pt: *m/z* 759.943. Observed: *m/z* 760.343. Cyclic voltammetry: **6e** – e⁻ → [6e]¹⁺, +0.65 V. Anal. Calcd for C₃₆H₄₀N₂S₂Pt: C, 56.90; H, 5.31; N, 3.69. Found: C, 52.53; H, 4.71; N, 3.28.

[(Ph₂C₂S₂)Pt(CN^tBu)₂][SbCl₆], [6d][SbCl₆]. The following procedure was conducted under an atmosphere of Ar in oven-dried glassware. A solution of **6d** (0.119 g, 0.198 mmol) in dry CH₂Cl₂ (10 mL) cooled to –20° C was dropwise treated via cannula with a solution of tris(4-bromophenyl)ammoniumyl hexachloroantimonate (0.161 g, 0.197 mmol) in CH₂Cl₂ (10 mL) that was similarly chilled to –20° C and protected from ambient light with a wrapping of Al foil. A dark green color was immediately induced in the mixture. This reaction mixture was stirred at –20° C for 1 h in the dark, at which point the solvent was removed *in vacuo*. The residual dark solid was washed with Et₂O (3 x 5 mL) and dried under vacuum. Crystallization of [(Ph₂C₂S₂)Pt(CN^tBu)₂][SbCl₆]₂ as irregularly-shaped black crystals was accomplished by diffusion of Et₂O vapor into a CH₂Cl₂ solution held at –20° C under N₂. This salt is unstable in air, and in solution at room temperature it readily decomposes to [(Ph₂C₂S₂)₂Pt] within minutes of exposure to air. Yield: 0.064 g, 17.3%. The following solution spectroscopic data are pertinent a 2[6d]⁺ ↔ [6d]₂²⁺ equilibrium (*vide infra*) in which the former is believed to dominate: ¹H NMR (δ, ppm in CD₂Cl₂): 7.42–7.34 (overlapping m, 10H, aromatic C–H), 1.66 (s, 9H, ^tBu), 1.59 (s, 9H, ^tBu). IR (CH₂Cl₂, cm⁻¹): 2243 (vs, CN_{sym}), 2222 (vs, CN_{asym}). UV-vis absorption spectrum [CH₂Cl₂, λ_{max}, nm (ε_M, M⁻¹·cm⁻¹): ~439 (910), ~661 (1030), ~799 (4050).

[(Ph₂C₂S₂)Ni(CN^tBu)₂(μ-Ag)₂][BF₄]₂, [7][BF₄]₂. Under an atmosphere of Ar, a solution of AgBF₄ (0.029 g, 0.15 mmol) in CH₂Cl₂ (10 mL) was transferred via cannula to a solution of [(Ph₂C₂S₂)Ni(CN^tBu)₂] (0.070 g, 0.15 mmol) in dry CH₂Cl₂ (10 mL). The resulting mixture was stirred overnight in the dark at 25 °C under Ar. This magenta-colored solution was taken to dryness under reduced pressure, and the residual solid was washed with Et₂O (3 x 10 mL). Upon drying, a reddish-magenta solid product was collected. Diffraction quality crystals were obtained by slow diffusion of Et₂O vapor into a concentrated CH₂Cl₂ solution. Yield: 0.079 g, 80%. ¹H NMR (δ, ppm in CD₂Cl₂): 7.26–7.18 (m, 20H, aromatic C–H), 1.45 (s, 36H, ^tBu). IR (CH₂Cl₂, cm⁻¹): 2211 (vs, CN_{sym}), 2198 (vs, CN_{asym}). UV-vis absorption spectrum [CH₂Cl₂; λ_{max}, nm (ε_M, M⁻¹·cm⁻¹): 523 (~35).

[(2,6-Me₂py)Ni(μ₂-η¹,η¹-S',η¹-S''-C₂Ph₂)₂], 8. Via gas-tight syringe, 2,6-dimethylpyridine (0.500 mL, 4.32 mmol) was delivered dropwise to a solution of **4a** (0.050 g, 0.130 mmol) in toluene (25 mL) under an argon atmosphere. The mixture was refluxed for 2 h, after which time it was cooled to room temperature. The volume of the solution was reduced by ~2 mL under vacuum to aid in the removal of displaced MeNC ligand. Reflux in toluene was continued overnight, after which time a minimal quantity of silica gel was added to the flask. The dark green-brown slurry was then taken to dryness *in vacuo*. This dry-loaded silica was added to the top of a column packed as a silica slurry in hexanes. Elution with 1:1 CH₂Cl₂:hexanes moved a green band of [(Ph₂C₂S₂)₂Ni] followed by brownish-orange **8**. Following collection of [(Ph₂C₂S₂)₂Ni], the latter band was fully drawn from the column using 2:1 CH₂Cl₂:hexanes. This fraction was reduced to dryness under reduced pressure, and the residual solid was washed with *n*-pentane and dried further. Recrystallization was achieved by the diffusion of hexanes vapor into a 1,2-dichloroethane solution. Yield: 0.023 g, 22%. R_f = 0.168 (2:1 CH₂Cl₂:hexanes). ¹H NMR (δ, ppm in CD₂Cl₂): 7.16-7.10 (m, ~12H, aromatic C-H), 6.89-6.87 (m, ~2H, aromatic C-H), 6.75-6.66 (m, ~8H, aromatic C-H), 6.56-6.53 (m, ~2H, aromatic C-H), 6.43-6.40 (m, ~2H, aromatic C-H), 3.96 (s, 6H, -CH₃), 3.70 (s, 6H, -CH₃). UV-vis absorption spectrum [CH₂Cl₂; λ_{max}, nm (ε_M, M⁻¹·cm⁻¹): 272 (8670), 364 (2800), 482 (2230), 693 (260). Cyclic voltammetry (CV): **27** + e⁻ → [**27**]⁻, +0.05 V; [**27**] - e⁻ → [**27**]⁺, +0.67 V. Anal. Calcd for C₄₂H₃₈N₂S₄Ni₂: C, 61.79; H, 4.69; N, 3.43. Found: C, 61.20; H, 4.62; N, 3.45.

[(Ph₂C₂S₂)Ni(CNMe)(PMe₃)], 9. Trimethylphosphine (0.50 mL, 5.0 mmol) was delivered dropwise via a gas-tight syringe to a solution of **4a** (0.039 g, 0.100 mmol) in CH₂Cl₂ (20 mL), which immediately induce formation of a purple color. The resulting mixture was stirred overnight at 25°C, after which time the volume of solvent was reduced to ~5 mL *in vacuo*. Addition of ~10 mL Et₂O led to the precipitation of a purple solid. The solvent was removed by cannula filtration, and the solid was washed with Et₂O (3 x 5 mL) to remove unreacted phosphine. The product was dried *in vacuo* for 1 h and redissolved in a minimal volume of 1,2-dichloroethane. Filtration of this concentrated solution through Celite and slow introduction of hexanes via vapor diffusion under an inert atmosphere afforded purple crystals. Yield: 0.0227 g, 53%. R_f = 0.13 (2:1 CH₂Cl₂:hexanes). ¹H NMR (δ, ppm in CD₂Cl₂): 7.21-7.06 (overlapping m, 10H, aromatic C-H), 3.44 (s, 3H, C≡NCH₃), 1.56 (d, J_{PH} = 12Hz, 9H, -P(CH₃)₃). ¹³C NMR (δ, ppm in CD₂Cl₂): 142.3, 129.70, 129.68, 127.42, 127.36, 125.7, 15.7 (d, J_{PC} = 30 Hz, P(CH₃)₃). ³¹P NMR (δ, ppm in CD₂Cl₂): 3.74. IR (CH₂Cl₂, cm⁻¹): 2199 (vs, CN). UV-vis absorption spectrum [CH₂Cl₂, λ_{max}, nm (ε_M, M⁻¹·cm⁻¹): 564 (370).

[(Ph₂C₂S₂)Ni(CNMe)(PPh₃)], 10. A solid portion of triphenylphosphine (0.113 g, 0.431 mmol) was added to a 20 mL CH₂Cl₂ solution of **4a** (0.0413 g, 0.108 mmol), which caused an immediate color change from blue to green. The resulting mixture was stirred overnight at 25°C, after which time the solvent was removed under reduced pressure. The residual solid was purified by chromatography on a silica column

packed as a slurry in hexanes. Unreacted phosphine ligand was separated first by flash elution with 1:1 CH₂Cl₂:hexanes; continued elution with 2:1 CH₂Cl₂:hexanes moved the product as a green band. The solvent was removed under reduced pressure, and the remaining solids were washed with Et₂O. Redissolution in a minimal amount of 1,2-dichloroethane, filtration through Celite, and slow crystallization by the introduction of hexanes via vapor diffusion afforded green crystals of the product. Yield: 0.0177 g, 26%. R_f = 0.30 (2:1 CH₂Cl₂:hexanes). ¹H NMR (δ, ppm in CD₂Cl₂): 7.81-7.75 (m, 6H, aromatic C–H), 7.53-7.50 (m, 9H, aromatic C–H), 7.36 (m, 3H, aromatic C–H), 7.19-7.06 (overlapping m, 10H, aromatic C–H), 2.87 (s, 3H, C≡NCH₃). ³¹P NMR (δ, ppm in CD₂Cl₂): 30.46. IR (CH₂Cl₂, cm⁻¹): 2204 (vs, CN). UV-vis absorption spectrum [CH₂Cl₂, λ_{max}, nm (ε_M, M⁻¹ cm⁻¹): 348 (3900), 463 (210), 622 (190). Calcd for C₃₄H₂₈NPS₂Ni: *m/z* 604.402. Observed: *m/z* 604.285.

[((Ph₂C₂S₂)Ni(C≡NMe))₂(μ-dppb)], 11. Under an atmosphere of argon, a CH₂Cl₂ (10 mL) solution of 1,4-dppb (0.312 g, 0.699 mmol) in CH₂Cl₂ (10 mL) was added dropwise by cannulation to a solution of **4a** (0.135 g, 0.352 mmol) in CH₂Cl₂ (10 mL). The mixture was stirred at 25 °C for ~10 h, and progress of the reaction was attended by a change in color from blue to dark green. The solvent was then reduced in volume, and a minimal amount of silica was added to the flask. The resulting slurry was taken to dryness *in vacuo*. The dry-loaded silica was applied directly to the top of a column packed as a slurry in hexanes. Elution with 1:1 CH₂Cl₂:hexanes moved unreacted ligand from the column; continued elution with 2:1 CH₂Cl₂:hexanes brought forward a well-resolved blue band of [(Ph₂C₂S₂)₂Ni]. The desired [((Ph₂C₂S₂)Ni(C≡NMe))₂(μ-dppb)] was flushed from the column as a green band using 5% THF in CH₂Cl₂. The solvent was removed from the eluant under reduced pressure, and the solid residue was washed with ~15 mL pentane and dried under vacuum. The product was then dissolved in a minimal volume of CH₂Cl₂, filtered through a Celite pad and taken to dryness again. Crystallization was accomplished by slow diffusion of Et₂O vapor into a concentrated CH₂Cl₂ solution of the product. Yield: 0.097 g, 49%. R_f = 0.81 (5% THF:CH₂Cl₂). ¹H NMR (δ, ppm in CD₂Cl₂): 7.85-7.79 (m, ~6H, aromatic C–H), 7.74-7.69 (m, ~4H, aromatic C–H), 7.56-7.47 (m, ~10H, aromatic C–H), 7.19–7.06 (overlapping m, ~24H, aromatic C–H), 2.71 (s, 6H, CNCH₃). ³¹P NMR (δ, ppm in CD₂Cl₂): 30.72. IR (CH₂Cl₂, cm⁻¹): 2223 (sh), 2211 (vs, CN). UV-vis absorption spectrum [CH₂Cl₂; λ_{max}, nm (ε_M, M⁻¹·cm⁻¹): 468 (520), 618 (420). Cyclic voltammetry: **9** – 2e⁻ → [**9**]²⁺, +0.51 V; [**9**]²⁺ – 2e⁻ → [**9**]⁴⁺, +1.26 V.

[((Ph₂C₂S₂)Pd(CNMe))₂(μ-dppb)], 12. The synthesis and purification procedures were analogous to those used for **11** but with 0.105 g (0.244 mmol) of **5a** and 0.217 g (0.486 mmol) of the 1,4-dppb ligand utilized. Crystallization of the product by the diffusion of Et₂O vapor into a concentrated CH₂Cl₂ solution of **12** produced violet diffraction-quality crystals. Yield: 0.121 g, 81%. R_f = 0.77 (5% THF:CH₂Cl₂). ¹H NMR (δ, ppm in CD₂Cl₂): 7.76-7.68 (overlapping m, ~12H, aromatic C–H), 7.56-7.49 (overlapping m, ~12H, aromatic C–H), 7.19-7.16 (m, ~4H, aromatic C–H), 7.13-7.05 (m, ~16H, aromatic C–H), 2.87 (s,

6H, CNCH₃). ³¹P NMR (δ, ppm in CD₂Cl₂): 22.62. IR (CH₂Cl₂, cm⁻¹): ~2240 (sh), 2227 (vs, CN). UV-vis absorption spectrum [CH₂Cl₂, λ_{max}, nm (ε_M, M⁻¹·cm⁻¹): ~438 (890), ~543 (820). Cyclic voltammetry: **10** – 2e⁻ → [**10**]²⁺, +0.52 V; [**10**]²⁺ – 2e⁻ → [**10**]⁴⁺, +0.93 V.

[[**(Ph₂C₂S₂)Pt(CNMe)₂(μ-dppb)**], **13**. The synthesis and purification procedures were analogous to those employed for **11** but with 0.246 g (0.473 mmol) of **6a** and 0.422 g (0.945 mmol) of the 1,4-dppb ligand utilized. Diffusion of Et₂O vapor into a concentrated CH₂Cl₂ solution of **9** produced bright yellow, diffraction-quality crystals. Yield: 0.119 g, 36%. R_f = 0.75 (5% THF:CH₂Cl₂). ¹H NMR (δ, ppm in CD₂Cl₂): 7.80–7.73 (overlapping m, 8H, aromatic C–H), 7.57–7.46 (overlapping m, 8H, aromatic C–H), 7.20–7.10 (overlapping m, 28H, aromatic C–H), 3.48 (s, 6H, CNCH₃). ³¹P NMR (δ, ppm in CD₂Cl₂): 14.94 (s, J_{Pt-P} = 2655 Hz). IR (CH₂Cl₂, cm⁻¹): ~2237 (sh), 2222 (vs, CN). UV-vis absorption spectrum [CH₂Cl₂, λ_{max}, nm (ε_M, M⁻¹·cm⁻¹): 340 (11800). Cyclic voltammetry: **11** – 2e⁻ → [**11**]²⁺, +0.57 V; [**11**]²⁺ – 2e⁻ → [**11**]⁴⁺, +1.26 V.

[**Et₄N**]₂[**(Ph₂C₂S₂)Ni(CN)₂**], [**Et₄N**]₂[**15**]. The following is a better-yielding alternative to a preparation reported earlier.¹⁰ A solution of [Et₄N]₂[Ni(CN)₄] (0.035 g, 0.083 mmol) in 10 mL MeCN (10 mL) was added to a solution of **4a** (0.030 g, 0.078 mmol) in 10 mL MeCN, which produced a change in color from dark blue to maroon. The solution was stirred overnight under inert atmosphere, after which time the solution volume was reduced to ~3 mL. Addition of 10 mL Et₂O induced precipitation of a red solid. The Et₂O was decanted by use of a cannula, and the solid was dried *in vacuo* for 1 h. Redissolution in a minimal volume of MeCN, filtration through Celite, and slow crystallization by the introduction of Et₂O via vapor diffusion afforded red crystals of [Et₄N]₂[**15**]. Yield: 0.016 g, 0.026 mmol, 35%. ¹H NMR (δ, ppm in CD₃CN): 7.16–7.11 (m, 4H, aromatic C–H), 7.09–7.02 (m, 6H, aromatic), 3.36–3.29 (4, 16H, N(CH₂CH₃)₄⁺), 1.30 (t, J = ~5H, 24H, N(CH₂CH₃)₄⁺). ¹³C NMR (δ, ppm in CD₃CN): 145.0, 138.0, 131.1, 130.6, 128.9, 126.8, 53.8 (–CH₂–, Et₄N⁺), 8.4 (–CH₃, Et₄N⁺). IR (CH₃CN, cm⁻¹): 2111 (vs, CN_{sym}), 2099 (vs, CN_{asym}). UV-vis absorption spectrum [CH₂Cl₂, λ_{max}, nm (ε_M, M⁻¹·cm⁻¹): 489 (220), 378 (5380). Cyclic voltammetry: [**15**]²⁻ – e⁻ → [**15**]¹⁻, –0.07 V.

[**Et₄N**][**(Ph₂C₂S₂)Pd(CN)(CNMe)**], [**Et₄N**][**16**]. Under an atmosphere of Ar, [Et₄N][CN] (0.100 g, 0.64 mmol) was added to a solution of **5a** (0.138 g, 0.32 mmol) in CH₃NO₂ (25 mL) and the mixture was refluxed overnight with stirring. A gradual color change from red to dark orange was observed as the reaction progressed. After being cooled, the solution was then reduced in volume, and a minimal amount of neutral alumina (~1.0 g) was added to the flask. The resulting slurry was taken to dryness *in vacuo*. The dry-loaded alumina was applied directly to the top of a neutral alumina column packed as a slurry in 1:1 CH₂Cl₂:CH₃CN. The column was then eluted with this same solvent mixture. A red band of unreacted started material was collected followed by a well resolved dark orange band of [Et₄N][**16**], which was fully flushed from the column with 100% CH₃CN. The solvent was removed from the eluant *in vacuo*, and the

residue was washed with Et₂O (3×10 mL). The residual solid was then dissolved in a minimal volume of CH₃CN, and the resulting solution was filtered through a Celite pad and taken to dryness again. Crystallization of [Et₄N][**16**] was accomplished by slow diffusion of Et₂O vapor into a concentrated CH₃CN solution. Yield: 0.104 g, 59%. R_f = 0.69 (1:1 CH₂Cl₂:CH₃CN). ¹H NMR (δ, ppm in CD₃CN): 7.11–7.01 (m, 10H, aromatic C–H), 3.41 (s, 3H, CNCH₃), 3.16 (q, 8H, N(CH₂CH₃)₄⁺), 1.19 (t, 12H, N(CH₂CH₃)₄⁺). IR (CH₂Cl₂, cm⁻¹): 2227 (vs, C≡NMe), 2120 (s, C≡N). UV-vis absorption spectrum [CH₂Cl₂; λ_{max}, nm (ε_M, M⁻¹·cm⁻¹): 338 (9800), 535 (920). Cyclic voltammetry: [**16**]¹⁻ – e⁻ → [**16**], +0.27 V.

[Et₄N][(Ph₂C₂S₂)Pt(CN)(CNMe)], [Et₄N][**17**]. The same synthesis and purification procedures used in the synthesis of [Et₄N][**16**] were employed but with 0.060 g (0.38 mmol) of [Et₄N][CN] and 0.066 g (0.13 mmol) of **6a**. Diffraction quality crystals were obtained by slow diffusion of Et₂O vapor into a saturated CH₃CN solution of the reddish-orange product. Yield: 0.040 g, 49%. R_f = 0.74 (1:1 CH₂Cl₂:CH₃CN). ¹H NMR (δ, ppm in CD₂Cl₂): 7.17–7.11 (m, 4H, aromatic C–H), 7.10–7.03 (m, 6H, aromatic C–H), 3.38 (s, 3H, CNCH₃), 3.24 (q, 8H, N(CH₂CH₃)₄⁺), 1.26 (t, 12H, N(CH₂CH₃)₄⁺). ¹³C NMR (δ, ppm in CD₂Cl₂): 144.4 (C≡NR, C≡N), 135.5, 130.4, 127.6, 125.8, 125.7, 53.2 (N(CH₂CH₃)₄⁺), 30.2 (CNCH₃), 7.9 (N(CH₂CH₃)₄⁺). IR (CH₂Cl₂, cm⁻¹): 2219 (vs, C≡NMe), 2120 (s, C≡N). UV-vis absorption spectrum [CH₂Cl₂, λ_{max}, nm (ε_M, M⁻¹·cm⁻¹): 497 (1350). Cyclic voltammetry: [**17**]¹⁻ – e⁻ → [**17**], +0.26 V.

[(Ph₂C₂S₂)Ni(IPr)(CNMe)], **18**. The synthesis, purification and characterization of **18** have been described previously.¹⁰

[(Ph₂C₂S₂)Pd(IPr)(CNMe)], **19**. The synthesis and purification procedures were analogous to those used for **18** but with 0.050 g (0.116 mmol) of **5a** and 0.090 g (0.232 mmol) of IPr.¹⁰ Purification was accomplished by flash column chromatography from a silica column eluted with 2:1 CH₂Cl₂:hexanes followed by 100% CH₂Cl₂ to collect **19** as an orange fraction. Crystallization of **19** as orange needle crystals was accomplished by the diffusion of hexanes vapor into a concentrated 1,2-dichloroethane solution. Yield: 0.0465 g, 51%. R_f = 0.70 (5% THF:CH₂Cl₂). ¹H NMR (δ, ppm in CD₂Cl₂): 7.58 (t, *J* = 6 Hz, 2H, aromatic C–H), 7.40 (d, *J* = 6 Hz, 4H, aromatic C–H), 7.25 (s, 2H, carbene –CH=HC–), 7.06–6.97 (overlapping m, 10H, aromatic C–H), 3.24 (s, 3H, CNCH₃), 2.96 (septet, *J* = 6 Hz, 4H, IPr –CH(CH₃)₂), 1.40 (d, *J* = 6 Hz, 12H, IPr –CH(CH₃)₂), 1.16 (d, *J* = 6 Hz, 12H, IPr –CH(CH₃)₂). ¹³C NMR (δ, ppm in CD₂Cl₂): 177.7, 146.3, 144.4, 135.9, 130.7, 130.5, 130.3, 127.4, 127.3, 125.6, 125.4, 124.6, 29.3 (CNCH₃), 26.5 (IPr, –CH(CH₃)₂), 22.9 (IPr, –CH(CH₃)₂). IR (CH₂Cl₂, cm⁻¹): 2213 (vs, CN). UV-vis absorption spectrum [CH₂Cl₂, λ_{max}, nm (ε_M, M⁻¹·cm⁻¹): 470 (370). Cyclic voltammetry: **19** – e⁻ → [**19**]¹⁺, +0.33 V.

[(Ph₂C₂S₂)Pt(C(NMe)(IPr))(C≡NMe)], **20**. The scale of synthesis and procedure for purification were the same as those detailed for **19**. Crude **20** was purified by flash column chromatography from a silica column eluted with 2:1 CH₂Cl₂:hexanes followed by 5% THF:CH₂Cl₂ to flush it from the column as a dark yellow band. After removal of the eluting solvents, crystallization of **20** was accomplished by the diffusion

of hexanes vapor into a concentrated 1,2-dichloroethane solution. Yield: 0.0166 g, 19%. $R_f = 0.75$ (5% THF:CH₂Cl₂). ¹H NMR (δ , ppm in CD₂Cl₂): 7.56 (t, $J = \sim 8$ Hz, 2H, aromatic C–H), 7.32 (d, $J = \sim 8$ Hz, 4H, aromatic C–H) 7.14 (s, 2H, carbene –CH=HC–), 7.12–6.99 (overlapping m, 10H, aromatic C–H), 3.24 (s, 3H, –CH₃), 3.03 (s, 3H, –CH₃), 2.90 (septet, $J = \sim 6$ Hz, 4H, IPr –CH(CH₃)₂), 1.26 (d, $J = 6$ Hz, 12H, IPr –CH(CH₃)₂), 1.14 (d, $J = 6$ Hz, 12H, IPr –CH(CH₃)₂). IR (CH₂Cl₂, cm^{–1}): 2213 (vs, CN). UV-vis absorption spectrum [CH₂Cl₂, λ_{\max} , nm (ϵ_M , M^{–1}·cm^{–1}): 344 (7530). Cyclic voltammetry: **20** – e[–] → [**20**]¹⁺, +0.28 V.

[(Ph₂C₂S₂)Ni(CNMe)(C(NHMe)(NMe₂))], **21**. Under an Ar atmosphere, tetraisopropyl benzobisimidazolium dibromide (0.100 g, 0.20 mmol) was transferred into an oven-dried 100 mL Schlenk flask followed by NaH (0.020 g, 0.82 mmol) and a catalytic amount of potassium *tert*-butoxide introduced via the tip of a spatula. The flask was affixed to a Schlenk line, and the mixture of solids was suspended in dry THF (50 mL). The mixture was stirred at 25° C for ~14 h, during which time smooth bubbling of H₂ gas was observed. Separation of the deprotected carbene ligand from the insoluble materials in the mixture was achieved by filtration through a Schlenk frit padded with 1 inch of Celite. The filtrate was transferred dropwise via cannula into a Schlenk flask containing a solution of **4a** (0.08 g, 0.2 mmol) in dry THF (10 mL). The resulting mixture was stirred for 8 h at 25° C, during which time the color changed from dark blue to magenta and then to red. The solvent was removed *in vacuo*, and the red residual solid was washed with Et₂O (3 x 10 mL). After being dried under vacuum, **21** was crystallized in diffraction quality form by slow diffusion of CH₃O*t*Bu vapor into a concentrated 1,2-dichloroethane solution. Yield: 0.081 g, 90.7%. ¹H NMR (δ , ppm in CD₂Cl₂): 7.19–7.01 (overlapping m, 10H, aromatic C–H), 5.55 (br, 1H, –NHCH₃ carbene), 3.92 (s, 3H, –CH₃), 3.71 (d, $J = 6$ Hz, 3H, –NHCH₃ carbene), 3.35 (s, 3H, –CH₃), 2.94 (s, 3H, –CH₃). ¹³C NMR (δ , ppm in CD₂Cl₂): 204.9, 143.6, 143.3, 137.9, 136.8, 130.2, 130.0, 127.7, 127.6, 125.6, 47.6, 36.6, 36.5, 30.3. IR (CH₂Cl₂, cm^{–1}): 2197 (vs, CN). UV-vis absorption spectrum [CH₂Cl₂, λ_{\max} , nm (ϵ_M , M^{–1}·cm^{–1}): 510 (200). Cyclic voltammetry: **24** – e[–] → [**24**]¹⁺, +0.35 V.

Discussion

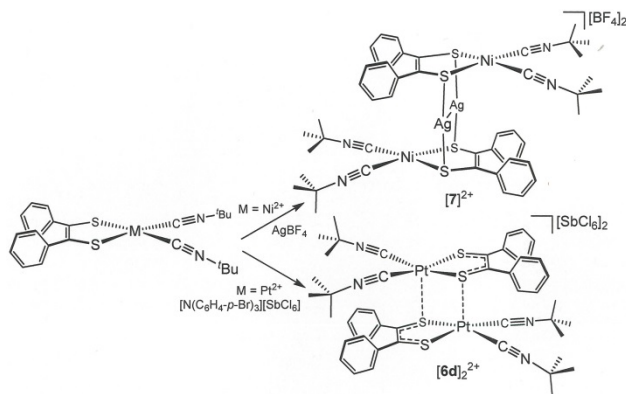
Synthesis and Structures. The formation of [(Ph₂C₂S₂)M(C≡NR)₂] from [(Ph₂C₂S₂)₂M] occurs readily under ambient conditions upon the introduction of 2 eq of C≡NR (**Scheme 3**, top). With constant metal (Ni²⁺) and isonitrile ligand (CN*t*Bu), variation in dithiolene ligand substituent among the set R' = Me, Ph, *p*-anisyl has no important effect upon either yield or upon physical properties (**Scheme 3**, bottom). These products are generally amenable to column chromatography purification and standard methods of crystallization.

In our preceding report,¹⁰ several members of the set **4a–4f**, **5a–5f** and **6a–6f** were described structurally (**4a**, **5d**, **6f**). In this succeeding work, the structures of the remaining members and of a variant with a different dithiolene ligand (**4bd**) are joined to the array to crystallographic data. Unit cell, refinement

Table 1. Selected bond lengths (Å), angles (deg.) for **4a-f**, **5a-f**, **6a-f**.^a

	4a	4b	4c^g	4d^h	4e	4f
Ni–C _{ave} ^b	1.8551[9] ^f	1.8454[13]	1.848[2]	1.8498(17)	1.848[2]	1.8507[13]
Ni–S _{ave}	2.1427[3]	2.1404[4]	2.1402[2]	2.1344(5)	2.1346[5]	2.1485[6]
Δ ^c	0.288	0.295	0.292	0.285	0.287	0.298
S–C _{ave}	1.7649[8]	1.7571[12]	1.761[2]	1.7577(16)	1.760[2]	1.7688[12]
C–C _{chelate}	1.348[1]	1.354(2)	1.346[3]	1.343(3)	1.351[3]	1.355(2)
C≡N _{ave}	1.149[1]	1.152[1]	1.149[2]	1.149(2)	1.147[2]	1.162[1]
C–Ni–C	89.91[5]	93.44(7)	90.68[11]	93.83(10)	89.15[10]	96.15(8)
S–Ni–S	90.478[13]	90.613(18)	91.10[3]	90.32(2)	90.79[3]	90.35(3)
S–Ni–C _{cis,ave}	90.18[3]	88.68[4]	89.87[5]	89.02(5)	90.60[5]	88.41[4]
S–Ni–C _{trans,ave}	173.44[3]	170.71[4]	169.13[5]	168.83(5)	171.51[5]	165.84[4]
θ, ^d deg.	6.5, 12.2	12.6	14.7, 19.9, 12.5	15.6	11.7, 13.4	19.2
δ, ^e Å	0.064, 0.121	0.127	0.147, 0.194, 0.121	0.155	0.113, 0.132	0.195
	5a	5b	5c	5d	5e	5f
Pd–C _{ave} ^b	2.002[1] ^f	1.994[2]	1.9982[11]	1.9955(13)	1.9945[2]	2.0010[13]
Pd–S _{ave}	2.2684[1]	2.2708[4]	2.2650[3]	2.2604(3)	2.2625[5]	2.2641[4]
Δ ^c	0.266	0.277	0.267	0.265	0.268	0.263
S–C _{ave}	1.762[1]	1.761[1]	1.7652[9]	1.7606(12)	1.765[2]	1.7668[11]
C–C _{chelate}	1.351(3)	1.352(3)	1.3555(17)	1.351(2)	1.347(3)	1.356(2)
C≡N _{ave}	1.135[2]	1.145[2]	1.1442[14]	1.1465(17)	1.145[3]	1.146[1]
C–Pd–C	91.8[4] ⁱ	92.07(1)	88.48(6)	93.33(7)	96.79(10)	92.20(7)
S–Pd–S	88.87(2)	88.940(19)	88.678(12)	88.028(16)	88.76(2)	88.356(15)
S–Pd–C _{cis,ave}	89.6[3] ⁱ	89.63[5]	91.44[3]	89.92(4)	87.27[5]	90.76[4]
S–Pd–C _{trans,ave}	175.7[2] ⁱ	175.52[5]	178.64[3]	171.28(4)	175.27[5]	175.13[4]
θ, ^d deg.	2.3, 8.7 ^j	5.5	1.9	11.7	3.3	4.4
δ, ^e Å	0.083, 0.024	0.059	0.020	0.123	0.036	0.044
	6a	6b	6c	6d	6e	6f
Pt–C _{ave} ^b	1.955[2] ^f	1.973[2]	1.964[3]	1.965[2]	1.957[2]	1.965[3]
Pt–S _{ave}	2.2757[5]	2.2829[6]	2.2747[7]	2.2773[5]	2.2745[6]	2.2748[7]
Δ ^c	0.321	0.310	0.311	0.312	0.318	0.310
S–C _{ave}	1.765[2]	1.760[2]	1.762[2]	1.763[2]	1.760[2]	1.764[3]
C–C _{chelate}	1.349[4]	1.353(4)	1.353(3)	1.343(4)	1.353(4)	1.345(5)
C≡N _{ave}	1.146[3]	1.134[3]	1.136[3]	1.145[3]	1.150[3]	1.138[4]
C–Pt–C	91.38[11]	91.43(12)	88.36(16)	96.13(12)	96.08(13)	90.70(7)
S–Pt–S	88.74[2]	89.13(3)	88.77(3)	89.12(2)	88.84(3)	91.512(17)
S–Pt–C _{cis,ave}	89.97[6]	89.78[6]	91.45[8]	87.37[6]	87.58[7]	89.99[4]
S–Pt–C _{trans,ave}	177.67[6]	178.51[6]	178.50[6]	176.27[6]	175.66[7]	176.67[4]
θ, ^d deg.	3.7, 1.6	4.1	2.1	1.9	3.2	4.0
δ, ^e Å	0.039, 0.013	0.044	0.021	0.008	0.034	0.041

^aThe structures of **4a**, **5d**, and **6f** were reported previously.⁷ Structural data are included here to assist identification of general trends. ^bUncertainties are propagated according to Taylor, J. R. *An Introduction to Error Analysis*; 2nd ed.; University Science Books: Sausalito, CA, 1997, pp 73-77. ^cΔ = M–S_{ave} – M–C_{ave}; ^dθ = angle between C–M–C and S–M–S planes; ^eAverage atom displacement from MS₂C₂ mean plane; ^fSquare brackets designate propagated uncertainty; ^gValues are from one whole molecule and two half molecules on special positions in the unit cell. ^hValues are not averaged, as only a half molecule occurs in the asymmetric unit of the cell. ⁱHigh uncertainties originate from the presence of a disordered MeNC, which was used in averaging. ^jTwo values occur due to a MeNC ligand disordered over two positions.



Scheme 4. Outcomes from reaction of $[(\text{Ph}_2\text{C}_2\text{S}_2)\text{M}(\text{CN}^t\text{Bu})_2]$ with oxidizing agents.

indices and other pertinent crystallographic data are available in supporting information (**Tables S1-S4**), while representative structures are depicted in **Figure 1**. Selected bond lengths and angles, presented where possible as averaged values, are gathered into **Table 1**. Considered in the aggregate, these data identify several trends: **1**) A tendency toward greater planarity, as gauged by θ , the angle between the MS_2 and MC_2 planes, and by δ , the average atom displacement (\AA) from the MS_2C_2 mean plane, upon descending the Group 10 metals from Ni to Pd to Pt (**Table 1**). This progression is due to the stronger ligand field enjoyed by the 2nd and 3rd row metals, in a constant ligand environment, as compared to a first row metal. **2**) A lower value of Δ , the difference between M-S and M-C bond lengths, in moving from Ni to Pd and then an increase in moving from Pd to Pt. This change arises from either an enhanced Pd-S interaction or diminished Pd-C bonding - or both - relative to the Ni and Pt compounds. **3**) A modest decrease in the isocyanide $\text{C}\equiv\text{N}$ bond length in moving from Ni^{2+} to Pd^{2+} to Pt^{2+} at parity of ligand such that, in more instances than not, the difference in $\text{C}\equiv\text{N}$ for the nickel compound vs the platinum compound is significant by the 3σ criterion (**Table 1**, bold type). The meaningfulness of this trend is corroborated by ν_{CN} (*vide infra*), which trend to higher energy as metal varies from Ni^{2+} to Pd^{2+} to Pt^{2+} .

Compounds of the type $[(\text{Ph}_2\text{C}_2\text{S}_2)\text{M}(\text{C}\equiv\text{NR})_2]$ generally support a single one-electron oxidation at $\sim+0.50$ V vs. AgCl/Ag (*vide infra*), which is attributed to transformation of the ene-1,2-dithiolate to radical monoanion (**Scheme 1**). Among redox agents with oxidizing power nominally sufficient to generate cationic $[(\text{Ph}_2\text{C}_2\text{S}_2)\text{M}(\text{C}\equiv\text{NR})_2]^+$ is Ag^+ in CH_2Cl_2 .¹⁹ Introduction of AgBF_4 in CH_2Cl_2 to $[(\text{Ph}_2\text{C}_2\text{S}_2)\text{Ni}(\text{C}\equiv\text{N}^t\text{Bu})_2]$ produces dimetallic $[(\text{Ph}_2\text{C}_2\text{S}_2)\text{Ni}(\text{C}\equiv\text{N}^t\text{Bu})_2]_2(\mu\text{-Ag})_2[\text{BF}_4]_2$ (**[7][BF4]2**, **Scheme 4**), wherein two closely juxtaposed Ag^+ ions are flanked by the dithiolene sulfurs atoms of two parallel $[(\text{Ph}_2\text{C}_2\text{S}_2)\text{Ni}(\text{C}\equiv\text{N}^t\text{Bu})_2]$ units such that the midpoint of the Ag_2^{2+} unit coincides with an inversion center and only half of the overall assembly is structurally unique. Intraligand S-C and $\text{C-C}_{\text{chelate}}$ bonds in $[\text{7}]^{2+}$ (**Table 2**, **Scheme 1**) remain consistent with ene-1,2-dithiolate formulation of the ligand and indicate that electron transfer did not occur. Rather, the Ag^+ ions have simply been ensconced between the soft thiolate

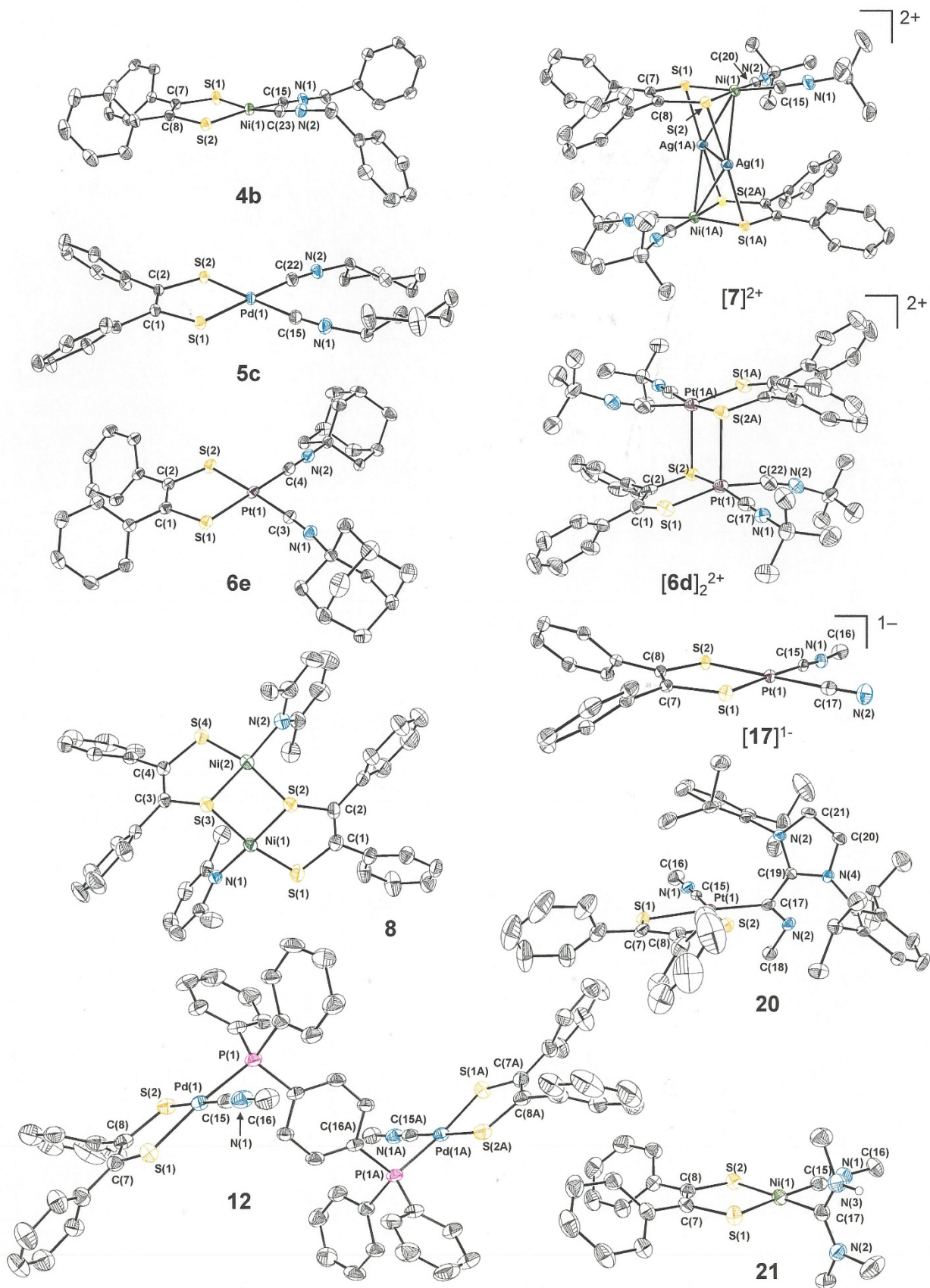


Figure 1. Representative thermal ellipsoid plots at the 50% probability level of compounds from Schemes 3, 4 and 5. Hydrogen atoms are omitted for clarity.

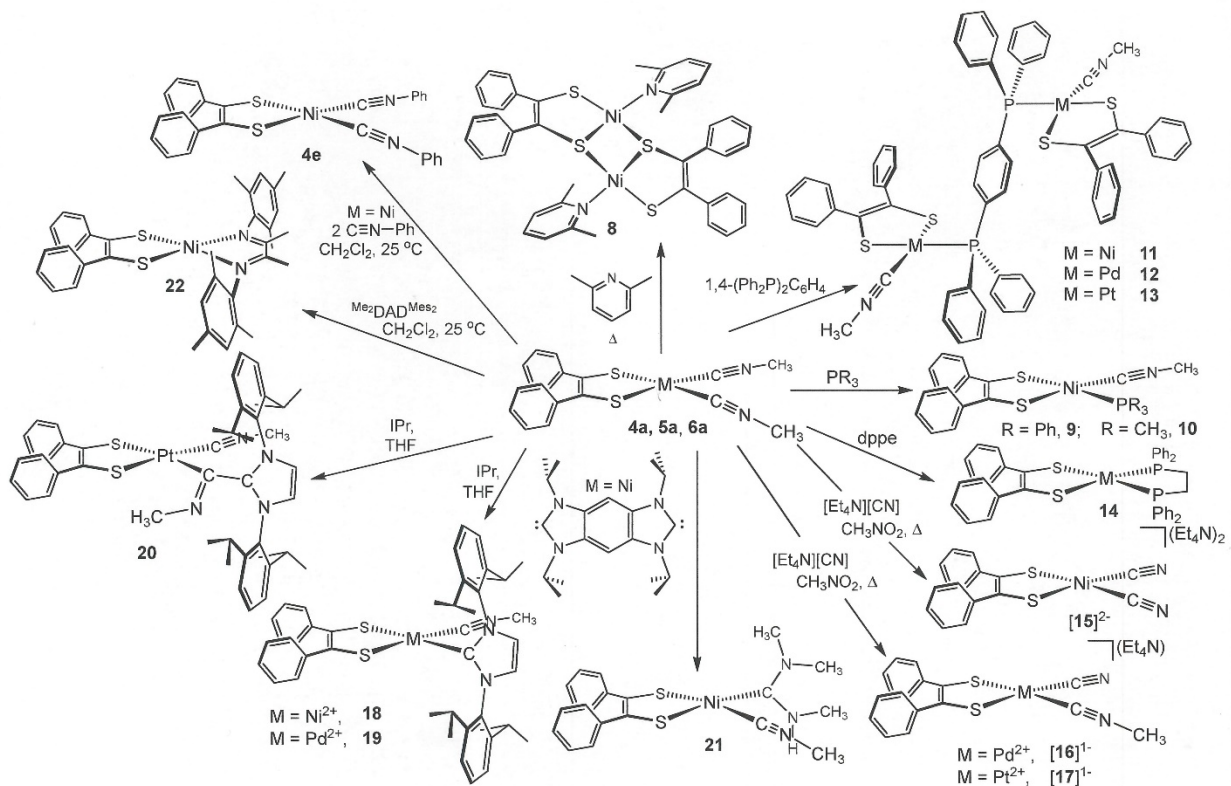
Table 2. Selected bond lengths (Å), angles (deg.) for [7]²⁺ and [6d]₂²⁺.

[7] ²⁺		[6d] ₂ ²⁺	
Ni–C _{ave}	1.863[2]	Pt–C ^d	1.986[7]
Ni–S _{ave}	2.1631[4]	Pt–C ^e	1.997[9]
Δ ^a	0.300	Pt–S ^f	2.263[1]
S–C _{ave}	1.7626[13]	Pt–S ^g	2.272[1]
C–C _{chelate}	1.348(2)	Δ ^a	0.276
C≡N _{ave}	1.146[2]	C≡N _{ave}	1.131[6]
S–Ag _{ave}	2.4403[4]	Pt...S ^h	2.749[1]
Ni–Ag _{ave}	2.9442[2]	S–C ⁱ	1.708[7]
Ag...Ag	3.0921(3)	S–C ^j	1.726[7]
Ni...Ni	5.011	C–C _{chelate}	1.384[9]
δ, ^b Å	0.054	δ, ^b Å	0.216, 0.223
C–Ni–C	92.94(9)	C–Pt–C	90.2[3]
S–Ni–S	90.877(19)	S–Pt–S ^k	87.70[6]
S–Ni–C _{cis,ave}	88.26[5]	S _{br} –Pt–S _{br} ^l	94.58[5]
S–Ni–C _{trans,ave}	173.85[4]	S _{non br} –Pt–S _{br} ^m	103.42[6]
Ag–Ni–Ag	63.352(7)	S–Pt–C _{trans, non br} ⁿ	162.4[2]
Ni–Ag–Ni	116.648(7)	S–Pt–C _{trans, br} ^o	173.1[2]
θ, ^c deg.	8.7	θ, ^c deg.	18.3, 18.9

^a Δ = M–S_{ave} – M–C_{ave}; ^b Displacement of M above the S₂C₂ mean plane. ^c θ = angle between C₂M and S₂M planes; ^d Isonitrile carbon *trans* to bridging sulfur; ^e Isonitrile carbon *cis* to bridging sulfur; ^f Dithiolene sulfur not involved in bridging; ^g Dithiolene sulfur involved in bridging; ^h Pt...S interaction through which dimerization occurs; ⁱ Dithiolene sulfur not involved in dimer formation; ^j Dithiolene sulfur involved in dimeric interaction; ^k Intraligand S–Pt–S angle; ^l Dithiolene sulfur atoms involved in bridging. ^m Angle defined by nonbridging sulfur and bridging dithiolene sulfur from other half of dimer; ⁿ *trans* S–Pt–C angle involving dithiolene sulfur not involved in bridging; ^o *trans* S–Pt–C angle involving dithiolene sulfur involved in bridging.

sulfur atoms. A similar outcome was found with [(dcpe)Ni(S₂C₆H₂S₂)Ni(dcpe)] (dcpe = 1,2-bis(dicyclohexylphosphino)ethane; [S₂C₆H₂S₂]⁴⁻ = 1,2,4,5-tetrathiolatobenzene) in reaction with Ag[B(3,5-(CF₃)₂-C₆H₃)₄]₂²⁰ and other complexes featuring the Ag₂²⁺ unit in an environment of sulfur donor atoms have been described.²¹⁻²²

Triarylammonium cations such as [N(C₆H₄-*p*-Br)₃]⁺ are both more potent oxidizing agents and uncomplicated by any tendency to act as ligand. Treatment of a CH₂Cl₂ solution of [(Ph₂C₂S₂)Pt(C≡N^tBu)₂] with [N(C₆H₄-*p*-Br)₃][SbCl₆] induces an immediate and pronounced darkening in color. Following removal of [N(C₆H₄-*p*-Br)₃] upon washing, recrystallization from CH₂Cl₂/Et₂O provides crystalline [(Ph₂C₂S₂)Pt(C≡N^tBu)₂]₂[SbCl₆]₂·2CH₂Cl₂ ([6d]₂[SbCl₆]₂·2CH₂Cl₂), which was identified by X-ray crystallography. Dimerization occurs via long Pt...S interactions (~2.75 Å, **Table 2**) that are enabled by moderate pyramidalization at the Pt²⁺ ions. This pyramidalization lifts the Pt²⁺ ions ~0.22 Å above the S₂C₂ mean plane and folds the PtS₂ and PtC₂ planes to a dihedral angle of ~18.5° from their near planarity in charge-neutral **6d** (**Table 2**). The center of the resulting Pt₂S₂ rhomb resides on an inversion center in triclinic *P*-1. Intraligand S–C and C–C_{chelate} bond lengths in [6d]₂²⁺ are appreciably shorter and longer, respectively, than the corresponding values in **6d** (*cf.* **Table 1**). These bond length changes indicate



Scheme 5. Substitution reactions of $[(\text{Ph}_2\text{C}_2\text{S}_2)\text{M}(\text{CNCH}_3)_2]$ ($\text{M} = \text{Ni}^{2+}, \text{Pd}^{2+}, \text{Pt}^{2+}$).

transformation of the dithiolene ligand from ene-1,2-dithiolate to radical monoanion (**Scheme 1**), which simultaneously introduces multiple bond character between sulfur and carbon and lowers the $\text{C}-\text{C}_{\text{chelate}}$ bond order. The general dimeric structure exemplified in $[\mathbf{6d}]_2^{2+}$ is typical for homoleptic $[\text{M}(\text{S}_2\text{C}_2\text{R}_2)_2]^{0,1-,2-}$ ($\text{M} = \text{Fe}, \text{Co}$) complexes²³⁻²⁴ but is a less common structure type for heteroleptic transition metal dithiolene complexes. A similar dimeric structure held by axial $\text{Pt}\cdots\text{S}$ interactions has been observed for $[\text{[(t-Bu-}p\text{-C}_6\text{H}_4)_2\text{C}_2\text{S}_2]\text{Pt}(4,4'\text{-t-Bu}_2\text{-bipy)}]_2[\text{PF}_6]_2$.²⁵

Following an initial limited set of observed displacements of MeNC from $[(\text{Ph}_2\text{C}_2\text{S}_2)\text{Ni}(\text{C}\equiv\text{NMe})_2]$,¹⁰ we have more thoroughly probed the breadth of substitution reactions that can be accomplished by new ligands across the $[(\text{Ph}_2\text{C}_2\text{S}_2)\text{M}(\text{C}\equiv\text{NMe})_2]$ ($\text{M} = \text{Ni}, \text{Pd}, \text{Pt}$) series. **Scheme 5** presents the full range of results observed thus far with $[(\text{Ph}_2\text{C}_2\text{S}_2)\text{M}(\text{C}\equiv\text{NMe})_2]$ ($\text{M} = \text{Ni}^{2+}, \text{Pd}^{2+}, \text{Pt}^{2+}$), including those disclosed previously. Treatment of **4a** with excess 2,6-dimethylpyridine led to modest yields of dimetallic **8**, which is noteworthy among the compounds of **Scheme 5** in being only one of two outcomes showing complete displacement of MeNC by a monodentate ligand. The two Ni^{2+} ions are bridged by one thiolate sulfur from each dithiolene ligand but in a slightly asymmetric fashion in which the shorter $\text{Ni}-\text{S}$ bond is formed with the sulfur atom from the dithiolene ligand that chelates the metal ion. The difference in $\text{Ni}-\text{S}_{\text{br}}$ bond lengths is ~ 0.07 (**Table 3**). The central Ni_2S_2 core shows a distinctive “butterfly” fold along the $\text{Ni}\cdots\text{Ni}$ axis such that the two $\text{Ni}-\text{S}_{\text{br}}-\text{Ni}$ planes meet at a 62.8° angle (**Figure 1**). The nearly planar $\text{C}_2\text{S}_2\text{Ni}$ metallodithiolene groups at the two ends of the molecule are, in consequence of the folding within the central Ni_2S_2 core,

Table 3. Selected interatomic distances (Å) and angles (deg.) for **8**.

	8
Ni···Ni	2.8406(9)
Ni–N	1.941[3]
Ni–S _{nonbridging}	2.1508[10]
Ni–S _{bridging, cis to N}	2.2158[10]
Ni–S _{bridging, trans to N}	2.1411[9]
Ni–S _{br} –Ni	81.36[3]
S _{br} –Ni–S _{br}	80.68[4]
S–Ni–S _{trans}	167.33[4]
S–Ni–S _{chelate}	89.72[4]
N–Ni–S _{br,trans}	174.09[9]
φ ^a , deg.	74.3
τ ^b , deg.	62.8

^aAngle between (C₂S₂)Ni coordination planes; ^bFold angle between Ni–S_{br}–Ni planes.

disposed at an angle of 74.3°. Similar structural features have been observed in dipalladium dithiolene complexes bearing Ph₃P in place of 2,6-dimethylpyridine.²⁶⁻²⁷

With either PPh₃ or PMe₃, substitution of MeNC in [(Ph₂C₂S₂)Ni(CNMe)₂] leads only to [(Ph₂C₂S₂)Ni(CNMe)(PPh₃)] (**9**) and [(Ph₂C₂S₂)Ni(CNMe)(PMe₃)₂] (**10**), both of which have been identified spectroscopically and structurally by X-ray diffraction. With the kinetic advantage of the chelate effect, 1,2-bis(diphenylphosphino)ethane (dppe) effects a second displacement of MeNC and produces [(Ph₂C₂S₂)Ni(dppe)] (**14**). An enhanced M–CNMe interaction is clearly manifested by a Ni–CNMe bond length that is shortened by ~0.03 Å relative to that in **4a** (*cf.* **Tables 1** and **4**) and by the greater resistance of this second isonitrile ligand to a second ligand substitution. As anticipated in view of the outcome found with PPh₃, use of 1,4-bis(diphenylphosphino)benzene with [(Ph₂C₂S₂)M(CNMe)₂] yields dimetallic [(Ph₂C₂S₂)M(CNMe)]₂(μ-1,4-(Ph₂P)₂C₆H₄) (M = Ni²⁺ (**11**), Pd²⁺ (**12**), Pt²⁺ (**13**)) (**Scheme 5, Figure 1**). Although crystals of **11-13** were grown under the same conditions, **11** crystallizes on a general position in triclinic *P*-1 with a *syn* disposition of the MeNC ligands, while **12** and **13** both occur on an inversion center in *P*-1, which demands an *anti* configuration of the two MeNC ligands. An upshot of the *syn* configuration in **11** is an intermetal distance that is ~1.3 Å shorter than in **12** and **13** (**Table 4**), while a consequence of the occurrence of **12** and **13** on inversion centers is a parallel disposition of the S₂MPC mean planes that contrasts with an angle of 67.4° for the square planar ends in **11**.

Table 4. Selected interatomic distances and angles in phosphine MeNC complexes.

	9	10	11	12	13
M–S ^a	2.1407(5)	2.1392(5)	2.1345[6] ⁱ	2.2727(9)	2.2780(10)
M–S ^b	2.1497(5)	2.1602(5)	2.1463[6]	2.2851(9)	2.2901(10)
Δ_{M-S}	0.009	0.021	0.0118	0.0124	0.0121
M–P	2.2025(5)	2.1908(5)	2.2028[6]	2.3210(9)	2.2881(10)
M–CNMe	1.8233(19)	1.8213(18)	1.826[2]	1.982(4)	1.958(4)
C≡N	1.155(3)	1.148(2)	1.153[3]	1.138(5)	1.130(5)
S–M–S	90.780(19)	91.045(18)	90.57[2]	88.00(3)	88.02(3)
C–M–P	93.36(6)	90.72(6)	91.16[6]	92.15(10)	90.62(11)
S–M–CNMe ^c	167.92(6)	177.74(6)	177.85[7]	176.20(10)	177.18(11)
S–M–P ^c	90.576(19)	89.737(19)	90.76[2]	91.46(3)	91.66(3)
S–M–CNMe ^d	88.06(6)	88.78(6)	87.54[6]	88.53(10)	89.86(11)
S–M–P ^d	166.47(2)	172.788(19)	177.07[3]	174.31(3)	174.95(3)
$\delta,^e \text{ \AA}$	0.187	0.078	0.010, 0.047	0.062	0.059
$\tau,^f \text{ \AA}$	-	-	7.848	9.138	9.162
$\theta,^g \text{ deg.}$	17.7	7.5	1.1, 4.9	5.7	5.4
$\varphi,^h \text{ deg.}$	-	-	67.4	0.0	0.0

^aS atom *trans* to MeNC; ^bS atom *trans* to phosphorus; ^cAngle defined with S atom *trans* to MeNC; ^dAngle defined with S atom *cis* to MeNC; ^eAverage atom displacement from MS₂CP mean plane; ^fDistance between M atoms; ^gAngle between MS₂ and MPC planes; ^hAngle between the two MS₂PC planes at each end of the dimetallic molecule. ⁱ[] notation designates uncertainties propagated in averaging.

Displacement of MeNC in [(Ph₂C₂S₂)Ni(CNMe)₂] by CN[−] can occur twice to afford [(Ph₂C₂S₂)Ni(CN)₂]^{2−} [**15**]^{2−}, but in poor yields of ~9%. The same dianion, however, is accessible in ~34% yield in the reaction between [Ni(CN)₄]^{2−} and [(Ph₂C₂S₂)Ni(CNMe)₂]. With [(Ph₂C₂S₂)M(CNMe)₂] (M = Pd or Pt), only monosubstitution to [(Ph₂C₂S₂)M(CN)(CNMe)]^{1−} occurs (M = Pd, [**16**]^{1−}; M = Pt, [**17**]^{1−}), evidently because enhanced dipositive character for the second and third metals provides for stronger metal–ligand bonding. Although no appreciable difference in M–CNMe bonds lengths exists between **5a** vs [**16**]^{1−} or **6a** vs [**17**]^{1−}, the M–S bond lengths in [**16**]^{1−} and [**17**]^{1−} reveal a modest difference of ~0.02 Å (**Table 5**) that suggests a slightly stronger *trans* influence for CN[−] over CNMe.

Compounds **4a** and **5a** undergo substitution of CNMe by IPr (IPr = 1,3-bis(2,6-diisopropylphenyl)imidazol-2-ylidene) to afford [(Ph₂C₂S₂)M(IPr)(CNMe)] (M = Ni, **18**; M = Pd **19**), the structures of which reveal a difference of 0.011–0.020 Å between M–S bond lengths (**Table 5**). This difference is in accord with a documented ligand field strength for Arduengo-type carbene ligands that is at least comparable to that of phosphines and CN^{1−}. Instead of simple ligand substitution, reaction between **6a** and IPr leads unexpectedly to a ketenimine-type ligand formed by attachment of the carbene carbon to the isonitrile carbon. The C–C_{ketenimine} bond length of 1.490[8] Å, which is indicative of single bond character, and an intraligand C–C–N angle of 113.0[4]°, which points toward *sp*² character for the carbon atom bound to Pt, are indicative of the charge separated resonance form of the ketenimine (**Scheme 6, (b)**) being the dominant contributor to its description. Insofar as Δ_{Pt-S} can be a gauge, (**Table 5**), the ketenimine ligand appears to be an appreciably stronger field ligand than even the Arduengo carbene. We are not aware of any prior example of this type of ligand in this binding mode. As reported by Bielawski,²⁸ the free

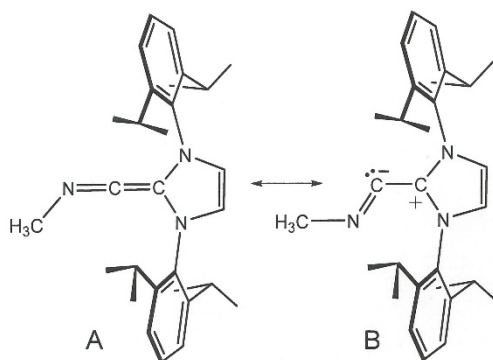
Table 5. Selected interatomic distances and angles in CN¹⁻, carbene, and ketenimine complexes.

	[16] ¹⁻	[17] ¹⁻	19	20 ^g	21
M–S ^a	2.2605(7)	2.2716(7)	2.2697(14)	2.272[1]	2.1292(8)
M–S ^b	2.2821(7)	2.2908(7)	2.2808(13)	2.317[1]	2.1625(8)
Δ _{M-S}	0.0216	0.0192	0.0111	0.045	0.033
M–CN, M–C _{carbene/ketenimine}	2.019(2)	1.993(2)	2.046(5)	2.057[6]	1.906(3)
M–CNMe	1.996(2)	1.953(3)	1.997(6)	1.948[6]	1.830(3)
C≡NMe	1.131(3)	1.140(3)	1.127(7)	1.135[7]	1.148(4)
C–C _{ketenimine}	-	-	-	1.490[8]	-
S–M–S	88.911(16)	88.858(18)	88.29(5)	88.86[5]	90.79(3)
C–M–C	92.50(7)	92.08(8)	92.9(5)	92.7[2]	89.47(13)
S–M–CNMe ^c	176.81(5)	177.86(7)	174.21(16)	178.3[2]	174.77(10)
S–M–CN ^c	177.78(6)	176.70(6)	-	-	-
S–M–C _{carbene/ketenimine} ^c	-	-	179.59(15)	175.4[1]	175.96(9)
S–M–CNMe ^d	90.42(5)	90.97(6)	86.72(16)	90.9[1]	94.41(9)
S–M–CN ^d	88.22(5)	88.14(6)	-	-	-
S–M–C _{carbene/ketenimine} ^d	-	-	92.09(14)	87.8[1]	85.32(9)
C–C–N _{ketenimine}	-	-	-	113.0[4]	-
C–N–CH _{3,ketenimine}	-	-	-	118.1[5]	-
δ, ^e Å	0.0267	0.0266	0.0252	0.0371, 0.0396	0.0064
θ, ^f deg.	2.5	2.5	2.9	3.4, 3.7	1.2

^aS atom *trans* to MeNC; ^bS atom *trans* to NC¹⁻ or carbene; ^cAngle defined with S atom *trans* to MeNC, NC¹⁻, or carbene; ^dAngle defined with S atom *cis* to MeNC, CN¹⁻, carbene, or ketenimine; ^eAverage atom displacement from MS₂CP mean plane; ^fAngle between MS₂ and MC₂ planes; ^gTwo independent molecules occur in the asymmetric unit. Values are averages of corresponding values from both molecules, and [] notation designates uncertainties propagated in averaging.

ketenimine that would be obtained by reaction of C≡N-^tBu and 1,3-bis(2,4,6-trimethylphenyl)imidazol-2-ylidene results in a similar angled geometry but faces unfavorable activation energetics. Carbene-derived ketenimines arising from direct reaction between isonitrile and carbene only appear accessible from electronically perturbed carbene derivatives such as *N,N'*-diamido substituted variants.²⁸

Use of tetraisopropylbenzobisimidazolium dibromide (**Scheme 5**), intended as a precursor to a bridging bis(carbene), in reaction with **4a** produced an unanticipated Fischer carbene ligand wherein the carbenoid carbon is asymmetrically flanked by NMe₂ and NHMe groups. The probable genesis of this ligand is via condensation of a free C≡NMe molecule with bound C≡NMe, with hydrogen atoms possibly originating from incompletely deprotected benzobisimidazolium dication or from adventitious moisture. In light of the

**Scheme 6.** Resonance forms of a ketenimine.



Scheme 7. Resonance forms of an isonitrile ligand.

well-documented capacity of carbenes to catalytically mediate a broad variety of carbon-carbon bond forming reactions,²⁹ this unanticipated outcome may involve the bis(carbene) complex activating either bound or free MeNC in a direct reaction, as opposed to accomplishing the intended straightforward substitution reaction. As gauged by the Δ_{M-S} values, the carbene ligand in **21** exerts a somewhat stronger *trans* influence than IPr, possibly because the larger steric profile of the latter tends to limit its bonding distance to M^{2+} . The asymmetry to the carbene ligand in **21** appears not to have a precedent, at least not in a structurally authenticated compound, but the symmetric noncyclic $C(NMe_2)_2$ carbene has been used in a few instances as a ligand in Group 11 complexes.³⁰⁻³¹

Spectroscopy. Compounds sets **4-6** exhibit two infrared stretching frequencies in the 2100-2300 cm^{-1} region, which arise from the symmetric and antisymmetric vibrations of the $C\equiv NR$ pair. These frequencies occur at *higher* energy than found for the free isonitrile (**Table 6**), indicating that π -backbonding is not

Table 6. Summary of infrared $C\equiv N$ stretching frequencies (cm^{-1}) in CH_2Cl_2 solution.

	Ni	Pd	Pt
$[(pdt)M(CNMe)_2]^a$ (2168) ^b	2228, 2214	2246, 2230	2248, 2223
$[(pdt)M(CNBn)_2]$ (2155) ^b	2213, 2197	2227, 2213	2229, 2204
$[(pdt)M(CNCy)_2]$ (2144) ^b	2204, 2189	2217, 2203	2219, 2196
$[(pdt)M(CN^tBu)_2]$ (2140) ^b	2197, 2180	2213, 2197	2214, 2188
$[(pdt)M(CN-1-Ad)_2]$ (2133) ^b	2196, 2175	2211, 2198	2212, 2192
$[(pdt)M(CNPh)_2]$ (2130) ^b	2182, 2162	2198, 2182	2199, 2172
$[(adt)M(CN^tBu)_2]^c$	2196, 2180	-	-
$[(mdt)M(CN^tBu)_2]^d$	2196, 2177	-	-
$[(pdt)M(CN^tBu)_2]^{1+}$	-	-	2243, 2222
$[\{(pdt)M(CN^tBu)_2\}_2(\mu-Ag)_2]^{2+}$	2211, 2198	-	-
$[(pdt)M(CNMe)(PMe_3)]$	2199	-	-
$[(pdt)M(CNMe)(PPh_3)]$	2204	-	-
$[(pdt)M(CNMe)_2(\mu-1,4-dppb)]$	2223, ^e 2211	2240, ^e 2227	2237, ^e 2222
$[(pdt)M(CN)_2]^{2-}$	2100, 2095 ^f	-	-
$[(pdt)M(CN)(CNMe)]^{1-}$	-	2227, 2120	2219, 2120
$[(pdt)M(IPr)(CNMe)]$	2190 ^f	2213	-
$[(pdt)M(C(NMe)(IPr))(CNMe)]$	-	-	2213
$[(pdt)M(C(NMe)(IPr))(CNMe)]$	2197	-	-

^apdt = $[Ph_2C_2S_2]^{2-}$; ^bValue for free ligand; ^cadt = $[(CH_3O-p-C_6H_4)_2C_2S_2]^{2-}$; ^dmdt = $[(CH_3)_2C_2S_2]^{2-}$; ^eShoulder; ^fData have been previously published.

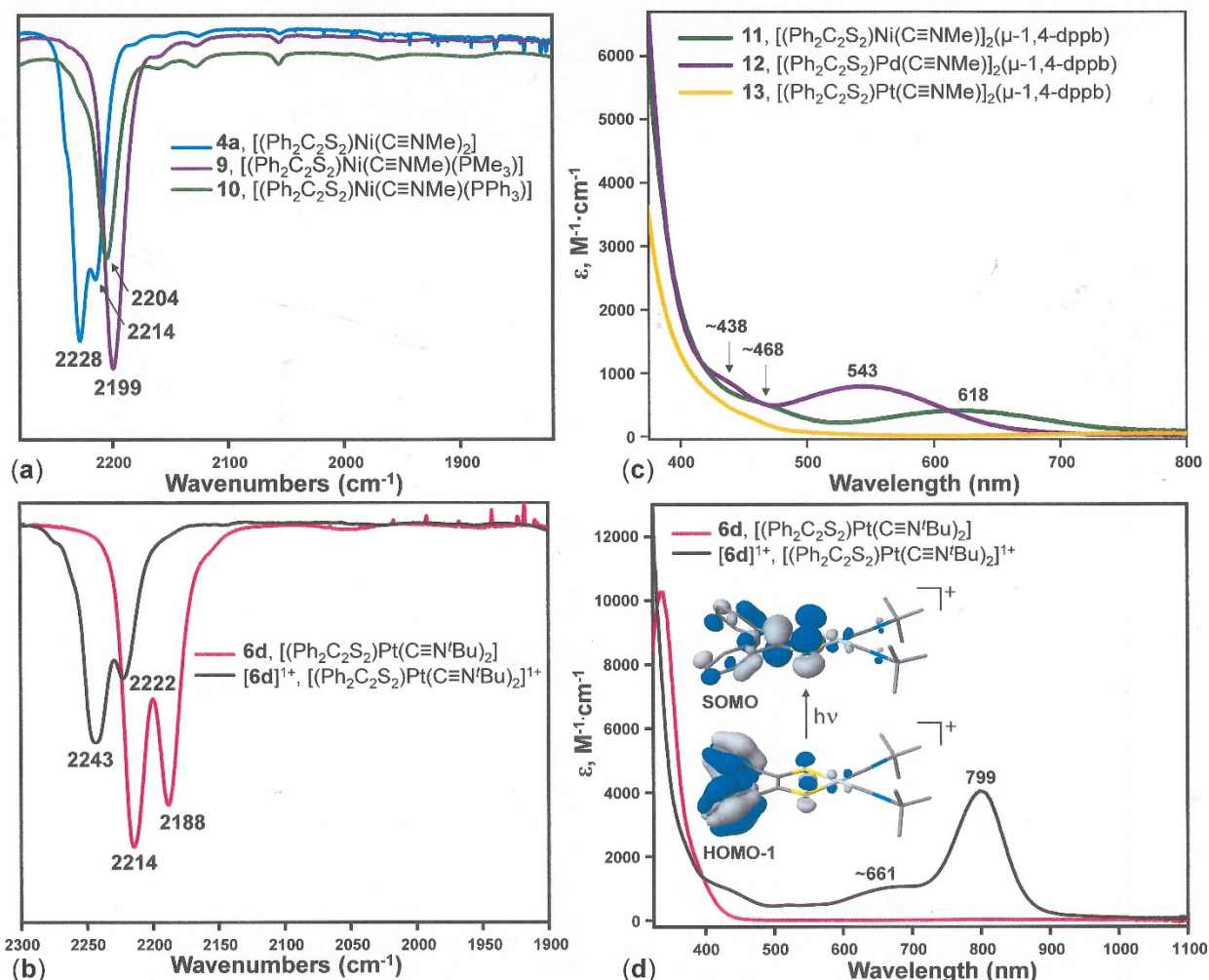


Figure 2. Selected IR ((a) and (b)) and UV-vis ((c) and (d)) spectra. The inset to panel (d) illustrates the MOs involved (0.04 contour level) with the 799 nm absorption.

relevant to the metal-ligand interaction and suggesting instead that the increase in stretching frequency arises from an increased importance of resonance form A relative to B (**Scheme 7**) when ligated to metal. These stretching frequencies increase as one traverses the series from Ni²⁺ to Pd²⁺ to Pt²⁺ at constancy of ligand, implying then an increasing positive character to the metal ion such that resonance form A is even further accentuated in its weighted contribution to the electronic description. A similar effect has been noted by Cotton in Group 10 isonitrile complexes.³² This behavior contrasts sharply with the 173-183 cm⁻¹ shift to lower energy observed for ν_{CN} in the zerovalent homoleptic isonitrile compounds [M(CN(2,6-Me₂C₆H₃))₆] (M = V,³³ W³⁴) and [M(CN(2,6-*i*-Pr₂C₆H₃))₆] (M = Nb,³⁵ Ta,³⁶ W³⁷), as compared to the free ligands. A decrease in ν_{CN} is found for **4-6** as R becomes more electron-donating (Me > Bn > Cy > ^tBu ≈ 1-Ad), while Ph produces the lowest value for ν_{CN} through a presumed delocalizing effect upon the isonitrile π -electrons.

Although π -backbonding does not describe the metal-isonitrile interaction in the compounds of **Schemes 3** and **4**, the isonitrile frequencies in $[(\text{Ph}_2\text{C}_2\text{S}_2)\text{M}(\text{CNMe})\text{L}]$ complexes manifest variation that apparently correlates to the σ donor power of L (**Figure 2 (a)**). Stronger σ -donors should moderate the positive character of M^{2+} and, because the negative end in charge-separated form A is then joined to metal ion with attenuated cationic charge, they should tend to promote resonance form B over A. The shift from 2204 to 2199 to 2190 cm^{-1} for ν_{CN} in moving from $[(\text{Ph}_2\text{C}_2\text{S}_2)\text{Ni}(\text{CNMe})(\text{PPh}_3)]$ to $[(\text{Ph}_2\text{C}_2\text{S}_2)\text{Ni}(\text{CNMe})(\text{PMe}_3)]$ to $[(\text{Ph}_2\text{C}_2\text{S}_2)\text{Ni}(\text{CNMe})(\text{IPr})]$ has a plausible basis in this light. In contrast,

Table 7. Summary of UV-vis spectral data for all compounds.

Compound	Electronic spectra, λ_{max} , nm (ϵ_{M} , $\text{M}^{-1}\cdot\text{cm}^{-1}$)
$[(\text{Ph}_2\text{C}_2\text{S}_2)\text{Ni}(\text{CNMe})_2]^a$	274 (31700), 348 (17200), 445 (240), 604 (300)
$[(\text{Ph}_2\text{C}_2\text{S}_2)\text{Ni}(\text{CNBn})_2]$	460 (400), 608 (420)
$[(\text{Ph}_2\text{C}_2\text{S}_2)\text{Ni}(\text{CNCy})_2]$	440 (240), 601 (420)
$[(\text{Ph}_2\text{C}_2\text{S}_2)\text{Ni}(\text{CN}^t\text{Bu})_2]$	424 (260), 600 (410)
$[(\text{MeO-}p\text{-C}_6\text{H}_4)_2\text{C}_2\text{S}_2]\text{Ni}(\text{CN}^t\text{Bu})_2]$	420 (200), 607 (320)
$[(\text{Me}_2\text{C}_2\text{S}_2)\text{Ni}(\text{CN}^t\text{Bu})_2]$	350 (6400), 450 (290), 614 (170)
$[(\text{Ph}_2\text{C}_2\text{S}_2)\text{Ni}(\text{CN-1-Ad})_2]$	437 (180), 599 (360)
$[(\text{Ph}_2\text{C}_2\text{S}_2)\text{Ni}(\text{CNPh})_2]$	466 (1400), 639 (480)
$[(\text{Ph}_2\text{C}_2\text{S}_2)\text{Pd}(\text{CNMe})_2]$	421 (690), 502 (530)
$[(\text{Ph}_2\text{C}_2\text{S}_2)\text{Pd}(\text{CNBn})_2]$	427 (150), 518 (50)
$[(\text{Ph}_2\text{C}_2\text{S}_2)\text{Pd}(\text{CNCy})_2]$	431 (430), 504 (490)
$[(\text{Ph}_2\text{C}_2\text{S}_2)\text{Pd}(\text{CN}^t\text{Bu})_2]^a$	240 (32500), 336 (17300), 419 (860), 498 (620)
$[(\text{Ph}_2\text{C}_2\text{S}_2)\text{Pd}(\text{CN-1-Ad})_2]$	430 (320), 505 (420).
$[(\text{Ph}_2\text{C}_2\text{S}_2)\text{Pd}(\text{CNPh})_2]$	385 (5180), 534 (770)
$[(\text{Ph}_2\text{C}_2\text{S}_2)\text{Pt}(\text{CNMe})_2]$	337 (4780)
$[(\text{Ph}_2\text{C}_2\text{S}_2)\text{Pt}(\text{CNBn})_2]$	342 (1560)
$[(\text{Ph}_2\text{C}_2\text{S}_2)\text{Pt}(\text{CNCy})_2]$	336 (9970)
$[(\text{Ph}_2\text{C}_2\text{S}_2)\text{Pt}(\text{CN}^t\text{Bu})_2]$	336 (10290)
$[(\text{Ph}_2\text{C}_2\text{S}_2)\text{Pt}(\text{CN-1-Ad})_2]$	336 (6850)
$[(\text{Ph}_2\text{C}_2\text{S}_2)\text{Pt}(\text{CNPh})_2]^a$	274 (35800), 390 (4070)
$[(\text{Ph}_2\text{C}_2\text{S}_2)\text{Pt}(\text{CN}^t\text{Bu})_2]^{1+}$	439 (910), 661 (1030), 799 (4050)
$[(\text{Ph}_2\text{C}_2\text{S}_2)\text{Ni}(\text{CN}^t\text{Bu})_2]_2(\mu\text{-Ag})_2]^{2+}$	523 (~35)
$[(2,6\text{-Me}_2\text{py})\text{Ni}(\mu_2\text{-}\eta^1, \eta^1\text{-S}^i, \eta^1\text{-S}^j, \eta^1\text{-S}^k\text{-C}_2\text{Ph}_2)]_2$	272 (8670), 364 (2800), 482 (2230), 693 (260)
$[(\text{Ph}_2\text{C}_2\text{S}_2)\text{Ni}(\text{C}\equiv\text{NMe})_2(\mu\text{-dppb})]$	468 (520), 618 (420)
$[(\text{Ph}_2\text{C}_2\text{S}_2)\text{Pd}(\text{C}\equiv\text{NMe})_2(\mu\text{-dppb})]$	438 (890), 543 (820)
$[(\text{Ph}_2\text{C}_2\text{S}_2)\text{Pt}(\text{C}\equiv\text{NMe})_2(\mu\text{-dppb})]$	340 (11800)
$[(\text{Ph}_2\text{C}_2\text{S}_2)\text{Ni}(\text{CNMe})(\text{PMe}_3)]$	564 (370)
$[(\text{Ph}_2\text{C}_2\text{S}_2)\text{Ni}(\text{CNMe})(\text{PPh}_3)]$	348 (3900), 463 (210), 622 (190)
$[(\text{Ph}_2\text{C}_2\text{S}_2)\text{Ni}(\text{CN})_2]^{2-}$	489 (220), 378 (5380)
$[(\text{Ph}_2\text{C}_2\text{S}_2)\text{Pd}(\text{CN})(\text{CNMe})]^{1-}$	338 (9800), 553 (920)
$[(\text{Ph}_2\text{C}_2\text{S}_2)\text{Pt}(\text{CN})(\text{CNMe})]^{1-}$	497 (1350)
$[(\text{Ph}_2\text{C}_2\text{S}_2)\text{Ni}(\text{IPr})(\text{CNMe})]^a$	350 (11600), 560 (410), 867 (120)
$[(\text{Ph}_2\text{C}_2\text{S}_2)\text{Pd}(\text{IPr})(\text{CNMe})]$	470 (370)
$[(\text{Ph}_2\text{C}_2\text{S}_2)\text{Pt}(\text{C}(\text{NMe})(\text{IPr}))(\text{CNMe})]$	344 (7530)
$[(\text{Ph}_2\text{C}_2\text{S}_2)\text{N}(\text{CNMe})(\text{C}(\text{NHMe})(\text{NMe}_2))]$	510 (200)

^aData have been previously published.

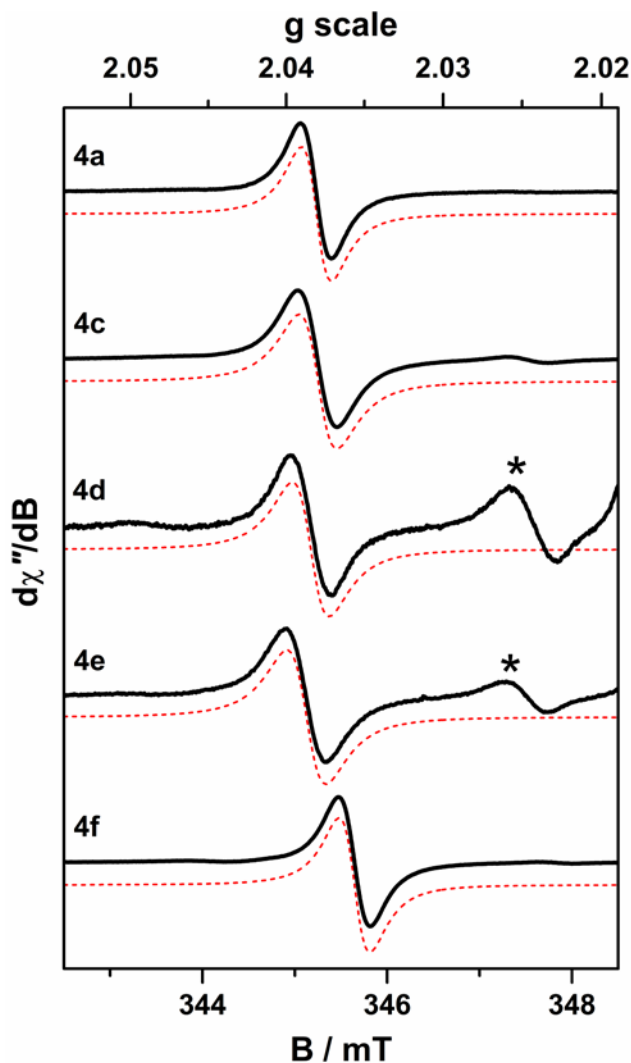


Figure 3. Comparison of the X-band EPR spectra of one-electron oxidized **4a** and **4c–4f** recorded in CH_2Cl_2 solution at 293 K (experimental conditions: frequency, 9.808 GHz; power, 6.3 mW; modulation, 0.5 mT). Experimental data are represented by the black line; simulation is depicted by the dashed trace: [**4a**]⁺, $g_{\text{iso}} = 2.0381$; [**4c**]⁺, $g_{\text{iso}} = 2.0383$; [**4d**]⁺, $g_{\text{iso}} = 2.0386$; [**4e**]⁺, $g_{\text{iso}} = 2.0386$; [**4f**]⁺, $g_{\text{iso}} = 2.0353$. The asterisk denotes an impurity caused by partial decomposition of the oxidized species at ambient temperature.

an effect of substantially greater magnitude is found for the $[(\text{acac})\text{Rh}(\text{CO})(\text{PR}_3)]$ series $\text{R} = \text{Ph}, \text{Cy},$ and Ad ($\nu_{\text{CO}} = 1977.6, 1958.7, 1948.3 \text{ cm}^{-1}$, respectively), where *bona fide* π -backbonding is likely operative.³⁸⁻
³⁹ For cationic $[(\text{Ph}_2\text{C}_2\text{S}_2)\text{Pt}(\text{CN}^t\text{Bu})_2]^+$, [**6d**]⁺, both symmetric and antisymmetric ν_{CN} shift to higher energy by $\sim 30 \text{ cm}^{-1}$ (**Table 6, Figure 2 (b)**) due to an amplification of the positive character at Pt^{2+} by oxidation of the dithiolene ligand to a monoanion and enhancement of structure A in **Scheme 7**. Structurally, in keeping with this increase in ν_{CN} , [**6d**]₂²⁺ shows a decrease in its average $\text{C}\equiv\text{N}$ bond length by $\sim 0.014 \text{ \AA}$ relative to **6d** (**Tables 1 and 2**). A more modest increase in ν_{CN} by $\sim 16 \text{ cm}^{-1}$ is observed for $[(\text{Ph}_2\text{C}_2\text{S}_2)\text{Ni}(\text{CN}^t\text{Bu})_2(\mu\text{-Ag})_2]^{2+}$ vs $[(\text{Ph}_2\text{C}_2\text{S}_2)\text{Ni}(\text{CN}^t\text{Bu})_2]$ since the positive charge, being associated with the Ag^{1+} ions, is less directly transmitted to the Group 10 metal.

The UV-vis spectra of compounds **4** feature low intensity absorptions at ~600 nm and at 420-460 nm, the former of which is a transition between the HOMO, comprised of the dithiolene π system, and the LUMO, which is M-L σ^* in nature and involves the metal $d_{x^2-y^2}$ atomic orbital. This band shifts to higher energy when M = Pd (~500 nm) and Pt (unresolved from other features at still higher energy) owing to the inherently higher energies of the d orbitals of the heavier metals (**Table 7**). The same pattern is evident in the mono(isonitrile) compounds of the type $[(\text{Ph}_2\text{C}_2\text{S}_2)\text{M}(\text{CNMe})\text{L}]$. As M varies from Ni to Pd to Pt in $[(\text{Ph}_2\text{C}_2\text{S}_2)\text{M}(\text{CNMe})]_2(\mu\text{-}1,4\text{-dppb})$, for example, the lowest energy absorption similarly moves from 618 nm to 543 nm to a position unresolved from higher energy absorption above ~450 nm (**Figure 2, (c)**).

Oxidation of **6d** by one electron induces a dark color and the onset of an intense low energy maximum at ~799 nm with an unresolved shoulder at ~661 nm (**Figure 2 (d)**). Absorptions in the lower energy 900-1100 nm region are conspicuously absent. The related cation, $[(^t\text{Bu-}p\text{-C}_6\text{H}_4)_2\text{C}_2\text{S}_2]\text{Pt}(4,4'\text{-}^t\text{Bu}_2\text{-bipy})^+$ ($\lambda_{\text{max}} = 728$ nm) has been shown by Wiegardt and coworkers to be in thermal equilibrium with the dimeric dication $[(^t\text{Bu-}p\text{-C}_6\text{H}_4)_2\text{C}_2\text{S}_2]\text{Pt}(4,4'\text{-}^t\text{Bu}_2\text{-bipy})_2^{2+}$ ($\lambda_{\text{max}} = 1015$ nm) and to be favored at ambient temperature.²⁵ Considering the fundamental similarity between $[(^t\text{Bu-}p\text{-C}_6\text{H}_4)_2\text{C}_2\text{S}_2]\text{Pt}(4,4'\text{-}^t\text{Bu}_2\text{-bipy})^+$ and $[(\text{Ph}_2\text{C}_2\text{S}_2)\text{Pt}(\text{C}\equiv\text{N}^t\text{Bu})_2]^+$, the lack of any absorption feature at energy lower than 800 nm suggests that $[(\text{Ph}_2\text{C}_2\text{S}_2)\text{Pt}(\text{C}\equiv\text{N}^t\text{Bu})_2]^+$ is the dominant species in solution and that $[(\text{Ph}_2\text{C}_2\text{S}_2)\text{Pt}(\text{C}\equiv\text{N}^t\text{Bu})_2]_2^{2+}$, although the form identified in the crystalline state, is of negligible concentration in CH_2Cl_2 at 25 °C. Time-dependent DFT calculations upon $[(\text{Ph}_2\text{C}_2\text{S}_2)\text{Pt}(\text{C}\equiv\text{N}^t\text{Bu})_2]^+$ suggest that the 799 nm absorption is due to an intraligand dithiolene π (phenyl) $\rightarrow \pi$ (C_2S_2) excitation ((**Figure 2 (d)**, inset) and that the 661 nm band is similar in description but involves the HOMO-2 with a different constitution to its phenyl π character.

The one-electron oxidation generally observed for compound types **4-6** is predominantly based on the C_2S_2 π system of the dithiolene ligand and produces a delocalized radical monoanion that gives rise to an isotropic signal. The g value for this signal is subject to minor variation as function of the nature of the isonitrile substituent R (**Figure 3**). A slight shift to higher g values is found as R varies from Me to the more electron-rich ^tBu and 1-adamantyl, while a somewhat greater move to lower g value is observed when R = Ph. As noted earlier in the context of $\text{C}\equiv\text{N}$ stretching frequencies, the Ph π -system exerts a modest delocalizing influence upon the $\text{C}\equiv\text{N}$ multiple bond; indirectly therefrom, the Ph group registers more effect upon the dithiolene radical than its aliphatic counterparts.

Electrochemistry. Compounds sets **4, 5, and 6** display a reversible or quasireversible one-electron oxidation that is due to the $\text{Ph}_2\text{C}_2\text{S}_2^{2-} \rightarrow \text{Ph}_2\text{C}_2\text{S}_2^{\cdot-} + e^-$ transformation. Consistent with the increasing positive character at metal that is indicated by ν_{CN} stretching frequencies (*vide supra*), the potentials for these oxidations (E_{ox}) trend toward more positive values as M varies from Ni to Pd to Pt (**Table 8**). Where available, data for $[(\text{Ph}_2\text{C}_2\text{S}_2)\text{M}(\text{CNMe})\text{L}]$ (L = phosphine, carbene) show E_{ox} that move toward less positive values as the donor strength of L increases and renders the oxidation more facile. Thus, E_{ox} values

Table 8. Summary of cyclic voltammetry data for [(pdt)M(L₁)(L₂)] in CH₂Cl₂ with [ⁿBu₄N][PF₆] supporting electrolyte. All waves are reversible except where noted otherwise. Potentials are referenced with respect to AgCl/Ag.^a

		M = Ni	M = Pd	M = Pt
MeNC	MeNC	+0.52	+0.61	+0.64
C ₆ H ₅ CH ₂ NC	C ₆ H ₅ CH ₂ NC	+0.50	+0.56	+0.57
CyNC	CyNC	+0.56	+0.61	+0.67
^t BuNC	^t BuNC	+0.59	+0.60	+0.66
^t BuNC	^t BuNC	+0.50 ^b	-	-
^t BuNC	^t BuNC	+0.42 ^c	-	-
1-Ad-NC	1-Ad-NC	+0.57	+0.59	+0.65
PhNC	PhNC	+0.62	+0.67	+0.73
2,6-Me ₂ py	μ ₂ -S-C ₂ Ph ₂ S	+0.05, +0.67 ^d	-	-
MeNC	1,4-(Ph ₂ P) ₂ C ₆ H ₄	+0.51, +1.26 ^e	+0.52, +0.93 ^d	+0.57, +1.26 ^d
CN ¹⁻	CN ¹⁻	-0.07	-	-
MeNC	CN ¹⁻	-	+0.27	+0.26
MeNC	IPr	+0.41, +1.78 ^e	+0.33	-
MeNC	C(NMe)IPr	-	-	+0.28
MeNC	C(NHMe)(NMe ₂)	+0.35	-	-

^a Under these conditions, the Cp₂Fe⁺/Cp₂Fe couple consistently occurred at +540 mV. ^bThe dithiolene ligand is [(CH₃O-*p*-C₆H₄)₂S₂C₂]²⁻ rather than [Ph₂C₂S₂]²⁻. ^cThe dithiolene ligand is [Me₂S₂C₂]²⁻ rather than [Ph₂C₂S₂]²⁻. ^dQuasireversible wave. ^eIrreversible wave.

for [(Ph₂C₂S₂)Ni(CNMe)]₂(μ-1,4-dppb), [(Ph₂C₂S₂)Ni(CNMe)(IPr)], and [(Ph₂C₂S₂)Ni(CNMe)(C(NHMe)(NMe₂))] trend as +0.51 V > +0.41 V > +0.35 V respectively. The basicity of the noncyclic carbene in **21** is likely greater than that of IPr in **18** because of a delocalizing effect of the imidazole ring in the latter. The electrochemistry of dimetallic compounds **11-13** is essentially similar to that of monometallic congeners **9** and **10** because their redox-active M(S₂C₂Ph₂) end groups are far enough apart as to be effectively independent. Thus, the waves they reveal at +0.51-0.57 V are attributed to concurrent one-electron oxidations of the metallodithiolene end-groups such that, as has been found for dimetallic compounds of the composition [(R₂C₂S₂)M(μ₂-tpbz)M(S₂C₂R₂)]⁴⁰⁻⁴¹ (tpbz = 1,2,4,5-tetrakis(diphenylphosphino)benzene), two remotely coupled radical monoanions are generated.

Compound **8** differs in kind from those of the type [(Ph₂C₂S₂)M(CNMe)L] in having no MeNC ligand. More importantly, while the compound is dimetallic, the bridging interactions are provided by a thiolate sulfur atom from each of the two dithiolene ligands. Consequently, the Ni₂(μ₂-η¹,η¹-S',η¹-S''-C₂Ph₂)₂ core can only be regarded as a single redox-active entity rather than as two independent fragments as in **11-13**. The cyclic voltammogram of **8** shows a reversible wave at +0.05 V, substantially less positive by ~+0.50 V than the oxidations found for compounds **4**. This feature is followed by a quasireversible oxidation at +0.67 V (**Figure 4**). As suggested by symmetry considerations and by its relatively compact core, the HOMO for **8** is largely composed of the C₂S₂ π systems of the two identical dithiolene ligands with modest contribution from Ni²⁺. Delocalization of charge in [**8**]¹⁺ throughout the Ni₂(μ₂-η¹,η¹-S',η¹-S''-C₂Ph₂)₂ center enables both the milder oxidation potential for **8** and, most likely, its capacity to sustain another oxidation

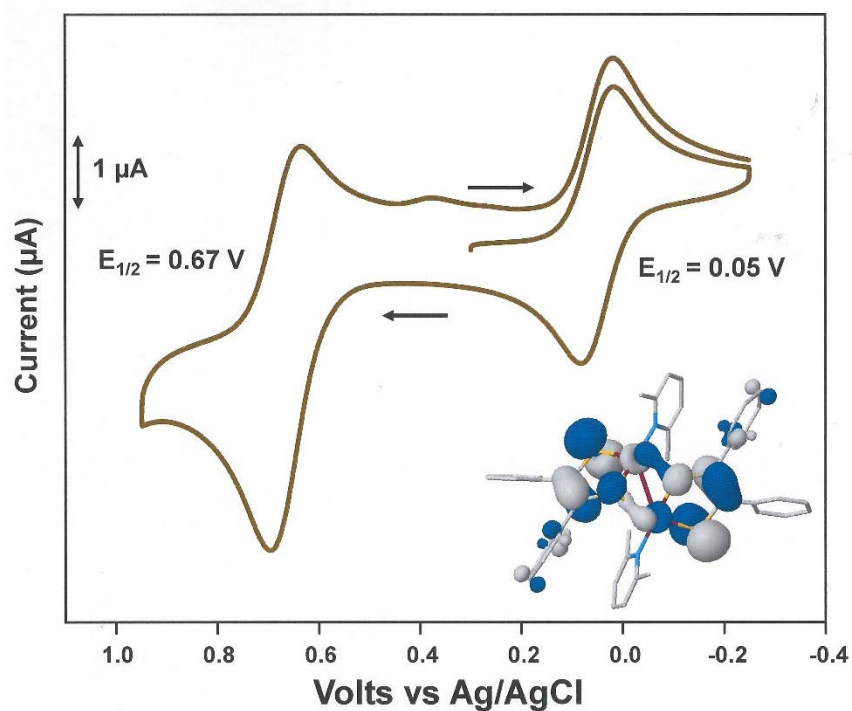


Figure 4. Cyclic voltammogram of $[(2,6\text{-Me}_2\text{py})\text{Ni}(\mu_2\text{-}\eta^1, \eta^1\text{-S}', \eta^1\text{-S}''\text{-C}_2\text{Ph}_2)_2]$ in CH_2Cl_2 with $[\text{Bu}_4\text{N}][\text{PF}_6]$ supporting electrolyte. The figure inset illustrates the HOMO (0.03 contour level), which is largely comprised of the C_2S_2 portions of the dithiolene ligands.

where compounds **4** cannot. Were it to be isolated, $[\mathbf{8}]^{1+}$ is anticipated to show $\text{C}-\text{C}_{\text{chelate}}$ and $\text{S}-\text{C}$ bond lengths between those of the fully reduced ene-1,2-dithiolate and the radical monoanion ((**a**) and (**b**), respectively, **Scheme 1**) since the presumed one-electron oxidation is averaged over two ligands. The LUMO for **8** is calculated as being ~ 2.8 eV higher in energy than the HOMO and, similar to compounds **4-6**, is $\text{M}(\text{d}_{x^2-y^2}) - \text{L} \sigma^*$ in nature.

Summary. The principal findings of this work are as follows:

(1) The synthesis of $[(\text{Ph}_2\text{C}_2\text{S}_2)\text{M}(\text{C}\equiv\text{NR})_2]$ ($\text{M} = \text{Ni}^{2+}, \text{Pd}^{2+}, \text{or Pt}^{2+}$; $\text{R} = \text{Me}, \text{Bn}, \text{Cy}, \text{'Bu}, 1\text{-adamantyl}, \text{Ph}$), proceed by dithiolene substitution from homoleptic $[(\text{Ph}_2\text{C}_2\text{S}_2)_2\text{M}]$. All compounds are air-stable and amenable to purification by column chromatography. Yields of isolated material range from 72-91% for $\text{M} = \text{Ni}^{2+}$, 55-80% for $\text{M} = \text{Pd}^{2+}$, and 37-52% for $\text{M} = \text{Pt}^{2+}$, implying stronger metal-dithiolene binding in moving from the first to the third row metal.

(2) Between this report and a preceding communication, all 18 members of the set have been characterized by X-ray crystallography. Progressively greater square planarity is observed in moving from Ni^{2+} to Pd^{2+} to Pt^{2+} .

(3) The ν_{CN} stretching frequencies in $[(\text{Ph}_2\text{C}_2\text{S}_2)\text{M}(\text{C}\equiv\text{NR})_2]$ all occur at higher energy than the free ligand and increase in energy as M varies from Ni^{2+} to Pd^{2+} to Pt^{2+} . This trend is rationalized as arising from increasing cationic character for the heavier metals, which tends to promote the linear, charge-separated resonance form of the isonitrile ligand ($\bar{\text{C}}\equiv\text{N}^+-\text{R}$) over its bent counterpart ($\text{:C}=\dot{\text{N}}-\text{R}$).

(4) Compound types $[(\text{Ph}_2\text{C}_2\text{S}_2)\text{M}(\text{C}\equiv\text{NR})_2]$ and $[(\text{Ph}_2\text{C}_2\text{S}_2)\text{M}(\text{C}\equiv\text{NR})\text{L}]$ sustain a reversible or quasireversible 1-electron oxidation due to the redox-active dithiolene ligand: $\text{Ph}_2\text{C}_2\text{S}_2^{2-} - \text{e}^- \rightarrow \text{Ph}_2\text{C}_2\text{S}^-\text{S}^\bullet$. In the case of $[(\text{Ph}_2\text{C}_2\text{S}_2)\text{Pt}(\text{C}\equiv\text{N}^t\text{Bu})_2]$, treatment with $[(\text{Br}-p\text{-C}_6\text{H}_4)_3\text{N}][\text{SbCl}_6]$ and crystallization of the isolated product yields centrosymmetric dimeric $[(\text{Ph}_2\text{C}_2\text{S}_2)\text{Pt}(\text{C}\equiv\text{N}^t\text{Bu})_2]_2^{2+}$ formed via $\text{Pt}\cdots\text{S}$ axial interactions in a rhombic $(\text{Pt}\cdots\text{S})_2$ core.

(5) The $[(\text{Ph}_2\text{C}_2\text{S}_2)\text{M}(\text{C}\equiv\text{NMe})_2]$ compounds provide access to new heteroleptic dithiolene compounds by displacement of $\text{MeN}\equiv\text{C}$ with various other ligands (CN^- , phosphine, carbene). The spectroscopic and electrochemical properties of $[(\text{Ph}_2\text{C}_2\text{S}_2)\text{M}(\text{C}\equiv\text{NMe})\text{L}]$ trend according to the σ -donor strength of L.

(6) Differences as function of M in the pattern of $\text{MeN}\equiv\text{C}$ displacement from $[(\text{Ph}_2\text{C}_2\text{S}_2)\text{M}(\text{C}\equiv\text{NMe})_2]$ arise from strengthened $\text{M}-\text{C}\equiv\text{NMe}$ binding in moving from $\text{M} = \text{Ni}^{2+}$ to Pd^{2+} to Pt^{2+} . Thus, for $\text{M} = \text{Ni}^{2+}$ and Pd^{2+} , the Arduengo carbene IPr reacts with $[(\text{Ph}_2\text{C}_2\text{S}_2)\text{M}(\text{C}\equiv\text{NMe})_2]$ to form $[(\text{Ph}_2\text{C}_2\text{S}_2)\text{M}(\text{IPr})(\text{C}\equiv\text{NMe})]$, while for $[(\text{Ph}_2\text{C}_2\text{S}_2)\text{Pt}(\text{C}\equiv\text{NMe})_2]$, IPr attacks the isonitrile carbon to form an $\eta^1, \kappa\text{C}$ -ketenimine ligand in a bent, charge-separated resonance form.

In continuing work, we probe the utility of $[(\text{Ph}_2\text{C}_2\text{S}_2)\text{M}(\text{C}\equiv\text{NMe})_2]$ as synthons toward new metallodithiolene compounds, including multi-metallic compounds, that are not accessible by other routes.

Associated Content

Supporting Information. Procedures for crystal growth, X-ray diffraction data collection, and structure solution and refinement; tables summarizing unit cell and refinement data (**Tables S1-S6**); thermal ellipsoid plots with complete atom labelling (**Figures S1- S48**); spectroscopic, electrochemical, and analytical data for compounds reported (**Figures S49-S196**); description of computation procedures; coordinates for geometry optimized structures.

Accession Codes. CCDC 1920776-1920790 and CCDC 1995894-1995907 contain the supplementary crystallographic data for this paper. These data can be obtained free of charge via www.ccdc.cam.ac.uk/data_request/cif, or by emailing data_request@ccdc.cam.ac.uk, or by contacting The Cambridge Crystallographic Data Centre, 12 Union Road, Cambridge CB2 1EZ, UK; fax: +44 1223 336033.

Author Information

Corresponding Authors

*E-mail: donahue@tulane.edu

Notes

The authors declare no competing financial interest.

Acknowledgments.

The Louisiana Board of Regents (LEQSF-(2002-03)-ENH-TR-67) and the National Science Foundation (MRI: 1228232 and 0619770) are thanked for funding of Tulane University's X-ray crystallography and mass spectrometry instrumentation, and Tulane University is acknowledged for its ongoing assistance with operational costs for the X-ray diffraction facility. The authors (A. O., J. P. D.) gratefully acknowledge support for this project from the National Science Foundation (CHE: 1836589). Ms. Titir Das Gupta is thanked for assistance with addressing a few experimental measurements.

References

- (1) Schrauzer, G. N.; Mayveg, V. P.; Heinrich, W. Coordination Compounds with Delocalized Ground States. α -Dithiodiketone-Substituted Group VI Metal Carbonyls and Related Compounds. *J. Am. Chem. Soc.* **1966**, *88*, 5174-5179.
- (2) Enemark, J. H.; Cooney, J. J. A.; Wang, J.-J.; Holm, R. H. Synthetic Analogues and Reaction Systems Relevant to the Molybdenum and Tungsten Oxotransferases. *Chem. Rev.* **2004**, *104*, 1175-1200.
- (3) Nomura, M.; Okuyama, R.; Fujita-Takayama, C.; Kajitani, M. New Synthetic Methods for η^5 -Cyclopentadienyl Nickel(III) Dithiolene Complexes Derived from Nickelocene. *Organometallics* **2005**, *24*, 5110-5115.
- (4) Adams, H.; Morris, M. J.; Morris, S. A.; Motley, J. C. Dithiolene Transfer from Nickel to a Dimolybdenum Centre: the First Dithiolene Alkyne Complex. *J. Organomet. Chem.* **2004**, *689*, 522-527.
- (5) Adams, H.; Gardner, H. C.; McRoy, R. A.; Morris, M. J.; Motley, J. C.; Torker, S. Heterometallic Dithiolene Complexes Formed by Stepwise Displacement of Cyclopentadienyl Ligands from Nickelocene with CpMo(S₂C₂Ph₂)₂. *Inorg. Chem.* **2006**, *45*, 10967-10975.
- (6) Adams, H.; Coffey, A. M.; Morris, M. J.; Morris, S. A. Efficient Transfer of Either One or Two Dithiolene Ligands from Nickel to Ruthenium: Synthesis and Crystal Structures of [Ru(SCR=CPhS)₂(PPh₃)] and [RuCl₂(SCR=CPhS)(PPh₃)₂] (R = Ph, H). *Inorg. Chem.* **2009**, *48*, 11945-11953.
- (7) Adams, H.; Grimes, L.; Morris, M. J.; Robertson, C. C. Dithiolene Transfer to the Molybdenum Nitrosyl Complex [CpMo(CO)₂(NO)]: Formation of Bimetallic Complexes. *J. Organomet. Chem.* **2018**, *87*, 73-79.
- (8) Adams, H.; Morris, M. J.; Robertson, C. C.; Tunnicliffe, H. C. I. Synthesis of Mono- and Diiron Dithiolene Complexes as Hydrogenase Models by Dithiolene Transfer Reactions, Including the Crystal Structure of [{Ni(S₂C₂Ph₂)₆}. *Organometallics* **2019**, *38*, 665-676.
- (9) Mayweg, V. P.; Schrauzer, G. N. Bis-adducts of Group VIII Metal Bisdithiobenzil Complexes with Phosphines. *Chem. Commun.* **1966**, 640-641.
- (10) Obanda, A.; Martinez, K.; Schmehl, R. H.; Mague, J. T.; Rubtsov, I. V.; Macmillan, S. N.; Lancaster, K. M.; Sproules, S.; Donahue, J. P. Expanding the Scope of Ligand Substitution from [M(S₂C₂Ph₂)₂] (M = Ni²⁺, Pd²⁺, Pt²⁺) to Afford New Heteroleptic Dithiolene Complexes. *Inorg. Chem.* **2017**, *56*, 10257-10267.
- (11) Hanson, G. R.; Gates, K. E.; Noble, C. J.; Griffin, M.; Mitchell, A.; Benson, S. XSophe-Sophe-XeprView®. A Computer Simulation Software Suite (v. 1.1.3) for the Analysis of Continuous Wave EPR Spectra. *J. Inorg. Biochem.* **2004**, *98*, 903-916.
- (12) Schuster, R. E.; Scott, J. E.; Casanova, J., Jr. Methyl Isocyanide. *Org. Synth.* **1966**, *46*, 75-77.
- (13) Eckert, H.; Nestl, A.; Ugi, I. Phenylisonitrile. In *Encyclopedia of Reagents for Organic Synthesis*; Wiley & Sons: 2001.
- (14) Gokel, G. W.; Widera, R. P.; Weber, W. P. Phase-Transfer Hofmann Carbylamine Reaction: *tert*-Butyl Isocyanide. *Org. Synth.* **1976**, *55*, 96-99.
- (15) Schmidtendorf, M.; Pape, T.; Hahn, F. E. Molecular Rectangles from Platinum(II) and Bridging Dicarbene, Diisocyanide, and 4,4'-Bipyridine Ligands. *Dalton Trans.* **2013**, *42*, 16128-16141.
- (16) Bantreil, X.; Nolan, S. P. Synthesis of *N*-Heterocyclic Carbene Ligands and Derived Ruthenium Olefin Metathesis Catalysts. *Nat. Protoc.* **2011**, *6*, 69-77.
- (17) Baldwin, R. A.; Cheng, M. T. Arylenebis(Tertiary Phosphines) and -(Phosphinic Acids. *J. Org. Chem.* **1967**, *32*, 1572-1577.
- (18) Amarego, W. L. F.; Perrin, D. D. Purification of Laboratory Chemicals, 4th ed; Butterworth-Heinemann: Oxford, U.K., 2000.
- (19) Connelly, N. G.; Geiger, W. E. Chemical Redox Agents for Organometallic Chemistry. *Chem. Rev.* **1996**, *96*, 877-910.

- (20) Arumugam, K.; Shaw, M. C.; Chandrasekaran, P.; Villagrán, D.; Gray, T. G.; Mague, J. T.; Donahue, J. P. Synthesis, Structures and Properties of 1,2,4,5-Benzenetetrathiolate Linked Group 10 Metal Complexes. *Inorg. Chem.* **2009**, *48*, 10591-10607.
- (21) Robertson, S. D.; Slawin, A. M. Z.; Woollins, J. D. Constructing Multimetallic Systems with the Naphthalene-1,8-bis(thiolato) Ligand. *Eur. J. Inorg. Chem.* **2007**, 247–253.
- (22) Shin, R. Y. C.; Tan, G. K.; Koh, L. L.; Vittal, J. J.; Goh, L. Y.; Webster, R. D. Metallophilicity in Annular Ru₂M₂ Derivatives of (HMB)Ru^{II}(tpdt) versus Bis-η²-Dithiolate Bonding in Ru₂M Derivatives of Cp*⁺Ru^{III}(tpdt) (HMB = η⁶-C₆Me₆; Cp* = η⁵-C₅Me₅; M = Cu^I, Ag^{I,II}, Au^I; tpdt = 3-thiapentane-1,5-dithiolate). *Organometallics* **2005**, *24*, 539–551.
- (23) Yu, R.; Arumugam, K.; Manepalli, A.; Tran, Y.; Schmehl, R.; Jacobsen, H.; Donahue, J. P. Reversible, Electrochemically Controlled Binding of Phosphine to Iron and Cobalt Bis(dithiolene) Complexes. *Inorg. Chem.* **2007**, *46*, 5131-5133.
- (24) Sproules, S.; Wieghardt, K. o-Dithiolene and o-Aminothiolate Chemistry of Iron: Synthesis, Structure and Reactivity. *Coord. Chem. Rev.* **2010**, *254*, 1358-1382.
- (25) Pap, J. S.; Benedito, F. L.; Bothe, E.; Bill, E.; DeBeer George, S.; Weyhermüller, T.; Wieghardt, K. Dimerization Processes of Square Planar [Pt^{II}(bpy)(dithiolato*)]⁺ Radicals. *Inorg. Chem.* **2007**, *46*, 4187-4196.
- (26) Pop, F.; Branzea, D. G.; Cauchy, T.; Avarvari, N. Bimetallic Neutral Palladium(II) Bis(dithiolene) Complex: Unusual Synthesis, Structural and Theoretical Study. *CR Chim.* **2012**, *15*, 904-910.
- (27) Chandrasekaran, P.; Greene, A. F.; Lillich, K.; Capone, S.; Mague, J. T.; DeBeer, S.; Donahue, J. P. A Structural and Spectroscopic Investigation of Octahedral Platinum Bis(dithiolene)phosphine Complexes: Platinum Dithiolene Internal Redox Chemistry Induced by Phosphine Association. *Inorg. Chem.* **2014**, *53*, 9192-9205.
- (28) Hudnall, T. W.; Moorhead, E. J.; Gusev, D. G.; Bielawski, C. W. *N,N'*-Diamidoketenimines via Coupling of Isocyanides to an *N*-Heterocyclic Carbene. *J. Org. Chem.* **2010**, *75*, 2763-2766.
- (29) Enders, D.; Niemeier, O.; Henseler, A. Organocatalysis by *N*-Heterocyclic Carbenes. *Chem. Rev.* **2007**, *107*, 5606-5655.
- (30) Coyle, J. P.; Sirianni, E. R.; Korobkov, I.; Yap, G. P. A.; Dey, G.; Barry, S. T. Study of Monomeric Copper Complexes Supported by *N*-Heterocyclic and Acyclic Diamino Carbenes. *Organometallics* **2017**, *36*, 2800-2810.
- (31) Holthoff, J. M.; Engelage, E.; Kowsari, A. B.; Huber, S. M.; Weiss, R. Noble Metal Corrosion: Halogen Bonded Iodocarbenium Iodides Dissolve Elemental Gold – Direct Access to Gold-Carbene Complexes. *Chem. Eur. J.* **2019**, *25*, 7480-7484.
- (32) Cotton, F. A.; Zingales, F. The Donor-Acceptor Properties of Isonitriles as Estimated by Infrared Study. *J. Am. Chem. Soc.* **1961**, *83*, 351–355.
- (33) Barybin, M. V.; Young, V. G., Jr.; Ellis, J. E. First Paramagnetic Zerovalent Transition Metal Isocyanides. Synthesis, Structural Characterizations, and Magnetic Properties of Novel Low-Valent Isocyanide Complexes of Vanadium. *J. Am. Chem. Soc.* **2000**, *122*, 4678-4691.
- (34) Lockwood, M. A.; Fanwick, P. E.; Rothwell, I. P. Reactivity of a Tungsten(II) Aryloxide with Isocyanides and Isocyanates. *Organometallics* **1997**, *16*, 3574-3575.
- (35) Kucera, B. E.; Roberts, C. J.; Young, V. G., Jr.; Brennessel, W. W.; Ellis, J. E. Niobium Isocyanide Complexes, Nb(CNAr)₆, with Ar = 2,6-Dimethylphenyl (Xyl), a Diamagnetic Dimer Containing Four Reductively Coupled Isocyanides, and Ar = 2,6-Diisopropylphenyl (Diip), a Paramagnetic Monomer Analogous to the Highly Unstable Hexacarbonylniobium(0). *Acta Crystallogr., Sect. C.* **2019**, *75*, 1259-1265.

- (36) Chakarawet, K.; Davis-Gilbert, Z. W.; Harstad, S. R.; Young, V. G., Jr.; Long, J. R.; Ellis, J. E. Ta(CNDipp)₆: An Isocyanide Analogue of Hexacarbonyltantalum(0). *Angew. Chem. Int. Ed.* **2017**, *56*, 10577-10581.
- (37) Sattler, W.; Ener, M. E.; Blakemore, J. D.; Rachford, A. A.; LaBeaume, P. J.; Thackeray, J. W.; Cameron, J. F.; Winkler, J. R.; Gray, H. B. Generation of Powerful Tungsten Reductants by Visible Light Excitation. *J. Am. Chem. Soc.* **2013**, *135*, 10614-10617.
- (38) Brink, A.; Roodt, A.; Steyl, G.; Visser, H. G. Steric vs. electronic anomaly observed from iodomethane oxidative addition to tertiary phosphine modified rhodium(I) acetylacetonato complexes following progressive phenyl replacement by cyclohexyl [PR₃ = PPh₃, PPh₂Cy, PPhCy₂, PCy₃]. *Dalton Trans.* **2010**, *39*, 5572-5578.
- (39) Chen, L.; Ren, P.; Carrow, B. P. Tri(1-adamantyl)phosphine: Expanding the Boundary of Electron-Releasing Character Available to Organophosphorus Compounds. *J. Am. Chem. Soc.* **2016**, *138*, 6392-6395.
- (40) Arumugam, K.; Shaw, M. C.; Mague, J. T.; Bill, E.; Sproules, S.; Donahue, J. P. Long-Range Spin Coupling: A Tetraphosphine-Bridged Palladium Dimer. *Inorg. Chem.* **2011**, *50*, 2995-3002.
- (41) Arumugam, K.; Selvachandran, M.; Obanda, A.; Shaw, M. C.; Chandrasekaran, P.; Caston Good, S. L.; Mague, J. T.; Sproules, S.; Donahue, J. P. Redox-Active Metallodithiolene Groups Separated by Insulating Tetraphosphinobenzene Spacers. *Inorg. Chem.* **2018**, *57*, 4023-4038.

For Table of Contents Use Only

